AD 282 208

SUPERSONIC PARACHUTE RESEARCH

Rudi J. Berndt

TECHNICAL DOCUMENTARY REPORT NO. ASD-TDR-62-236

May 1962

282 208

Retardation and Recovery Branch
Flight Accessories Laboratory
Aeronautical Systems Division
Air Force Systems Command
Wright-Patterson Air Force Base, Ohio

Project No. 6065, Task No. 606505

NOTICES

When Government drawings, specifications, or other data are used for any purpose other than in connection with a definitely related Government procurement operation, the United States Government thereby incurs no responsibility nor any obligation whatsoever; and the fact that the Government may have formulated, furnished, or in any way supplied the said drawings, specifications, or other data, is not to be regarded by implication or otherwise as in any manner licensing the holder or any other person or corporation, or conveying any rights or permission to manufacture, use, or sell any patented invention that may in any way be related thereto.

ASTIA release to OTS not authorized.

Qualified requesters may obtain copies of this report from the Armed Services Technical Information Agency, (ASTIA), Arlington Hall Station, Arlington 12, Virginia.

Copies of ASD Technical Reports and Technical Notes should not be returned to the Aeronautical Systems Division unless return is required by security considerations, contractual obligations, or notice on a specific document.

FOREWORD

This report was prepared by the Retardation and Recovery Branch, Flight Accessories Laboratory, Aeronautical Systems Division, and reflects the efforts being accomplished under Project 6065, Task 606505, "Parachute Performance in Supersonic Flow." The author presented this paper at the Short Term Summer Course on Aerodynamic Deceleration held at the University of Minnesota in July 1961.

The original applied research efforts upon which this report is based were, to a large degree, conducted by private industry and educational institutions under Air Force contract. The author, Rudi J. Berndt, served as project engineer for the Air Force program conducted under Project 6065.

ABSTRACT

Supersonic vehicles require aerodynamic deceleration systems that will function efficiently and predictably at supersonic speeds over a wide range of altitudes. Deceleration from supersonic speeds at high altitudes involves problems that require new approaches. To meet these greater requirements, extensive applied research is being conducted in the field of aerodynamic deceleration. This research is expected to provide information for designing adequate deceleration devices that will perform consistently so that recovery trajectories can be predicted.

Parachute canopies are being investigated since parachutes normally provide a high ratio of aerodynamic drag to weight and bulk. Reliable data exist for Guide-Surface and Flat Circular Ribbon parachute canopies at transonic speeds and dynamic pressures as great as 2500 lb/ft^2. At supersonic speeds, however, inflation has been erratic, drag forces reduced, and materials failed at a fraction of rated strength. Probable causes for this erratic behavior are discussed and promising modifications and designs of parachute canopies for supersonic operation are presented.

PUBLICATION REVIEW

TABLE OF CONTENTS

LIST OF ILLUSTRATIONS

LIST OF ILLUSTRATIONS (Continued)

INTRODUCTION

The number of applications and uses for aerodynamic deceleration devices has increased at an amazing rate during the past two decades. During World War II, these devices were used almost daily in large-scale operations for emergency and premiditated escape from aircraft and for aerial delivery of military supplies. Since World War II, however, the expanding capabilities of new vehicles has given rise to new applications for these devices that were then undreamed of.

Present aerodynamic deceleration devices, together with their associated initiating and actuating components, have become one of the most important subsystems in any vehicle of flight. Expanding applications have required new aerodynamic deceleration system concepts of more complex design and operation. Some of the new concepts are depicted in Figure 1. Establishing design criteria and performance characteristics of new deceleration systems has necessitated accelerated explorations in a new scientific field -- aerodynamic deceleration technology.

Extensive research and development efforts have been and are being undertaken and sponsored by the United States Air Force. The purpose of these research and development efforts is the advancement of the state-of-the-art of aerodynamic decelerator technology. Phenomena associated with the design and operation of aerodynamic deceleration devices to be used throughout the entire regime of flight are being explored and investigated. Based upon data obtained from these efforts, parameters will be developed for the design of aerodynamic deceleration devices and for predicting their performance for any present or future applications.

This report discusses the various applications and describes some of the different types of aerodynamic deceleration devices being considered for use with present and future flight vehicles. The main part of this report, however, deals with design criteria and performance characteristics of self-inflating trailing aerodynamic decelerators -- the conventional parachute canopy -- for operation in supersonic flight.

Manuscript released by the author in November 1961 for publication as an ASD Technical Documentary Report.

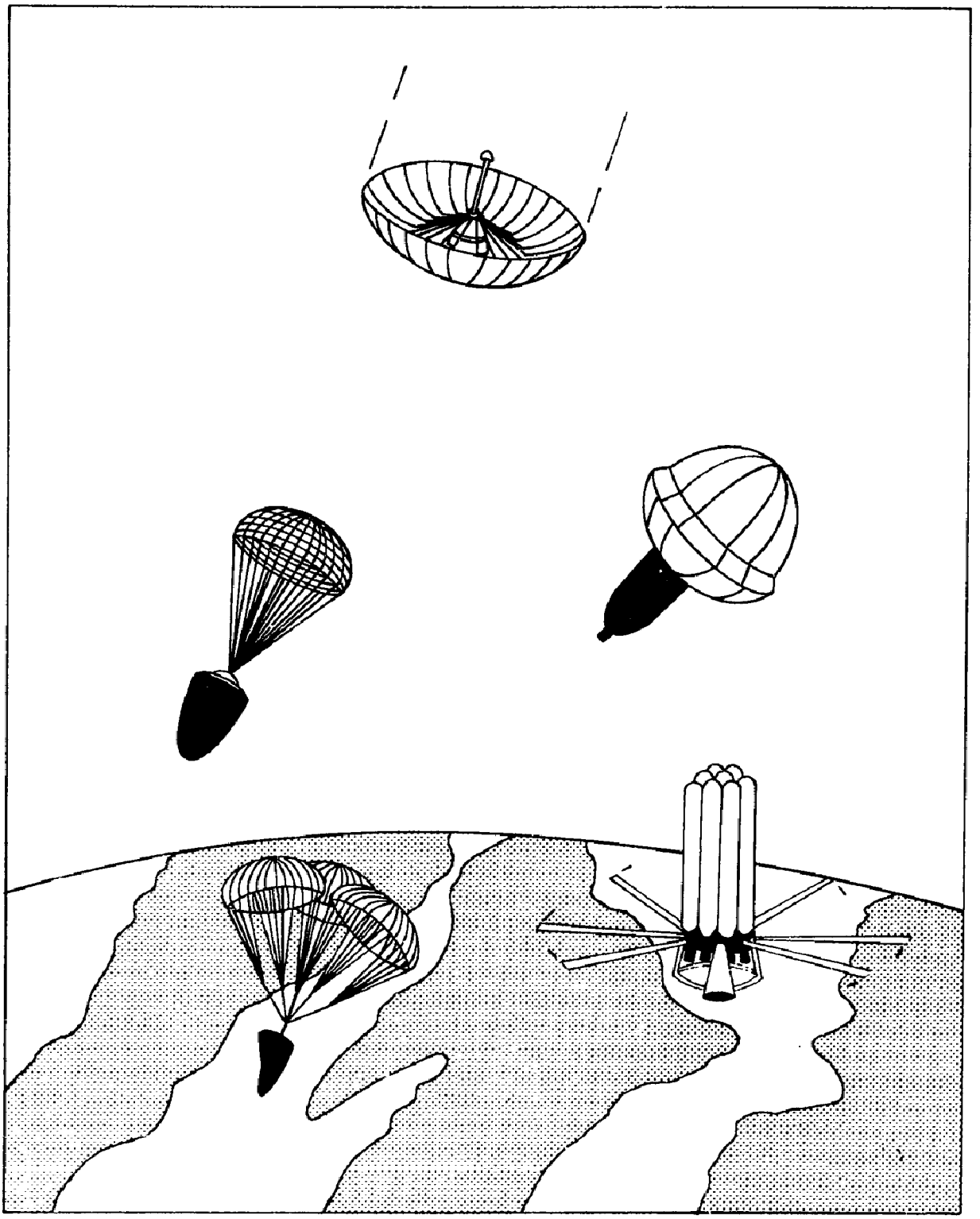

Figure 1. Deployable Aerodynamic Decelerators

AERODYNAMIC DECELERATION DEVICES

Aerodynamic decelerators, by virtue of their design configuration and performance characteristics, augment the basic aerodynamic drag and, in some cases, the stability of flight vehicles in a controllable manner. All aerodynamic drag devices generate a retarding force by changing the momentum of the air.

APPLICATIONS

The types of applications for aerodynamic deceleration devices can be divided according to the specific boundaries of the Mach number-altitude regime for the potential drag-device operations. The resulting operational flight spectrum can then be further divided to define the operational functions that may be required of the aerodynamic decelerator, as shown in Figure 2. We have divided the flight spectrum into three major application areas:

1. The subsonic-speed, low-altitude regime. Most applications for aerodynamic deceleration in the recovery or terminal operations of flight vehicles will naturally occur in this region.

2. The hypersonic-speed, low-dynamic-pressure regime. This region is bounded by two lines: (a) a line of equilibrium temperature of about 2000°F, above which the selection of materials becomes problematical; and (b) a line of constant dynamic pressure of 10 lb/ft^2, below which trajectory control by varying the aerodynamic drag becomes ineffective. Aerodynamic deceleration devices may be utilized throughout this flight regime to minimize re-entry aerodynamic heating, limit deceleration values, and control the final landing point for the vehicle.

3. The supersonic flight regime. This region is bounded by two lines of constant dynamic pressure: (a) an upper limit of 10,000 lb/ft^2, above which the structural problems of flexible drag devices may become insurmountable, and (b) a lower limit of 1.0 lb/ft^2, below which self-inflation of flexible drag devices becomes unreliable. In this region, therefore, pressure-inflated aerodynamic deceleration devices may have to be employed.

This report is concerned primarily with the supersonic flight regime.

AERODYNAMIC DRAG AUGMENTATION

Many aerodynamic drag augmentation devices have been employed as the mainstays for flight-vehicle deceleration in the supersonic flight regime. These devices have been selected because of their optimum drag-to-bulk or drag-to-weight ratios or because of their adaptability to stowage and attachment to the vehicles. Other devices are being considered for future applications. Methods for producing aerodynamic drag in the supersonic speed regime can be grouped into three broad categories; an example of each category is illustrated in Figure 3. These three categories and the problems associated with each are discussed as follows:

1. Utilization of devices that constitute an integral part of the flight-vehicle structure. This group includes dive brakes and body, leading-edge, and trailing-edge spoilers. Drag brakes and spoilers, in their usual deployment configuration, lie relatively close to the main body. At high Mach numbers, these devices lose effectiveness because of large dynamic pressure losses in the bow shock and shear-layer losses associated with the after-bodies of blunt-tipped bodies. When a vehicle is operated at high altitudes and high Mach numbers, these effects are aggravated because the shear layer becomes relatively thicker. In addition, airflow separates ahead of the drag brakes or spoilers when the vehicle is operated at supersonic Mach numbers, which further reduces their effectiveness.

2. Induced changes in vehicle configuration. Nose blunting by means of a programmed separation of a portion of the nose section of the vehicle is being used to augment the drag during initial phases of recovery operations. Increasing the bluntness will alter the flow

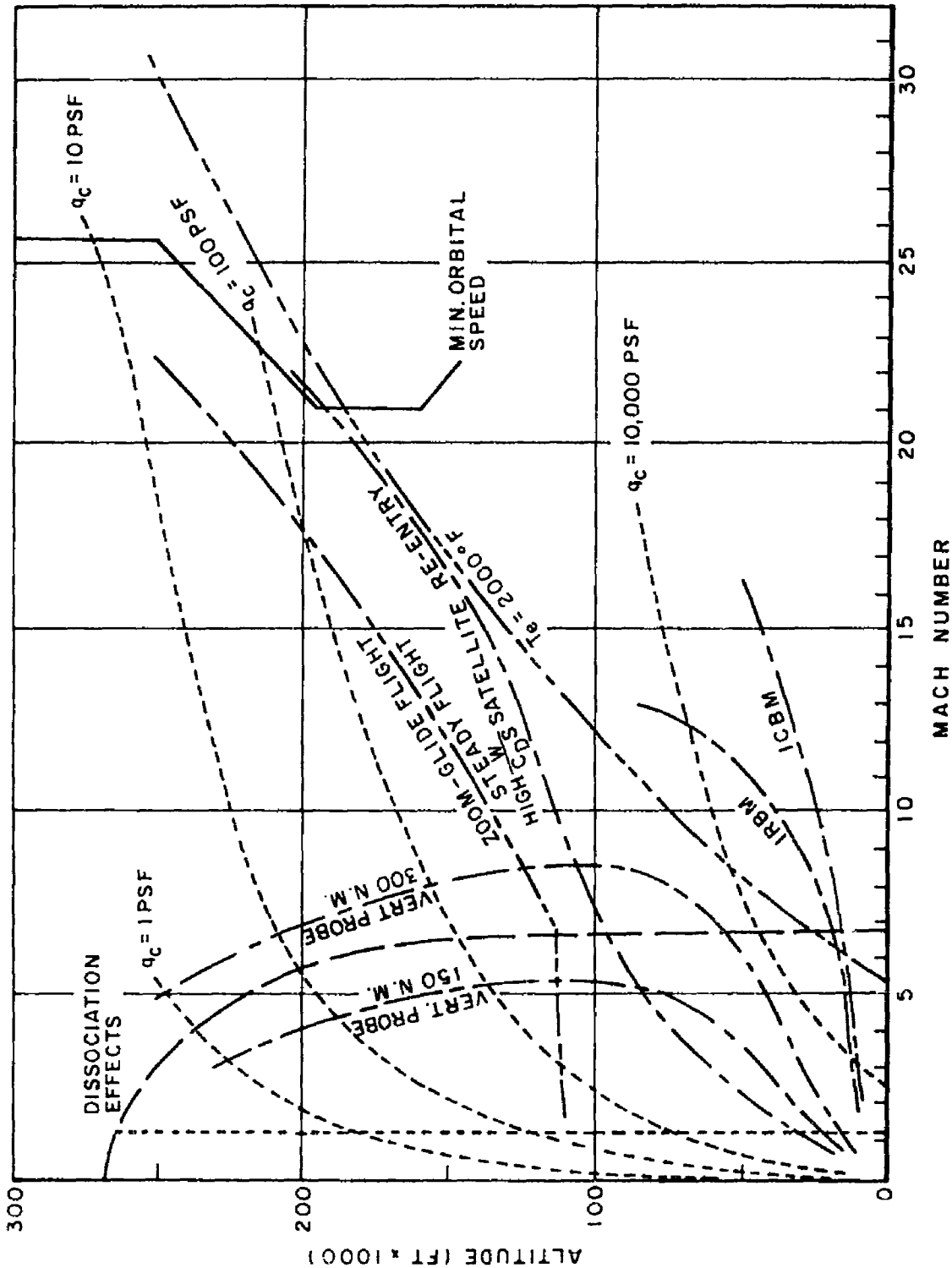

Figure 2. Altitude–Mach Number Regime

field and can effectively increase normal retarding forces; such blunt shapes are associated with unsteady flow, however, and produce undesirable yaw damping characteristics. These characteristics can aggrevate dynamic instability problems, particularly when dynamic pressure is reduced rapidly.

Modifying the flow field about the vehicle is an induced change that is being considered to agument aerodynamic deceleration. High supersonic flight produces temperatures that may be high enough to ionize the air about the vehicle sufficiently to produce magneto-aerodynamic effects. When a fluid is a conductor of electricity, an electric body force may be produced in that fluid to affect the flow pattern significantly. Before the magneto-aerodynamic effects can be applied to aerodynamic deceleration, however, we must consider the conductivity of the flow field and the required strength of the magnetic field. Obviously, generating a strong magnetic field would require a magnet of considerable weight.

3. Utilization of deployable drag devices that are not an integral part of the flight-vehicle structure. These devices may be either self-inflating or pressure-inflated; they may be attached directly to the flight vehicle or trailing the vehicle at some distance.

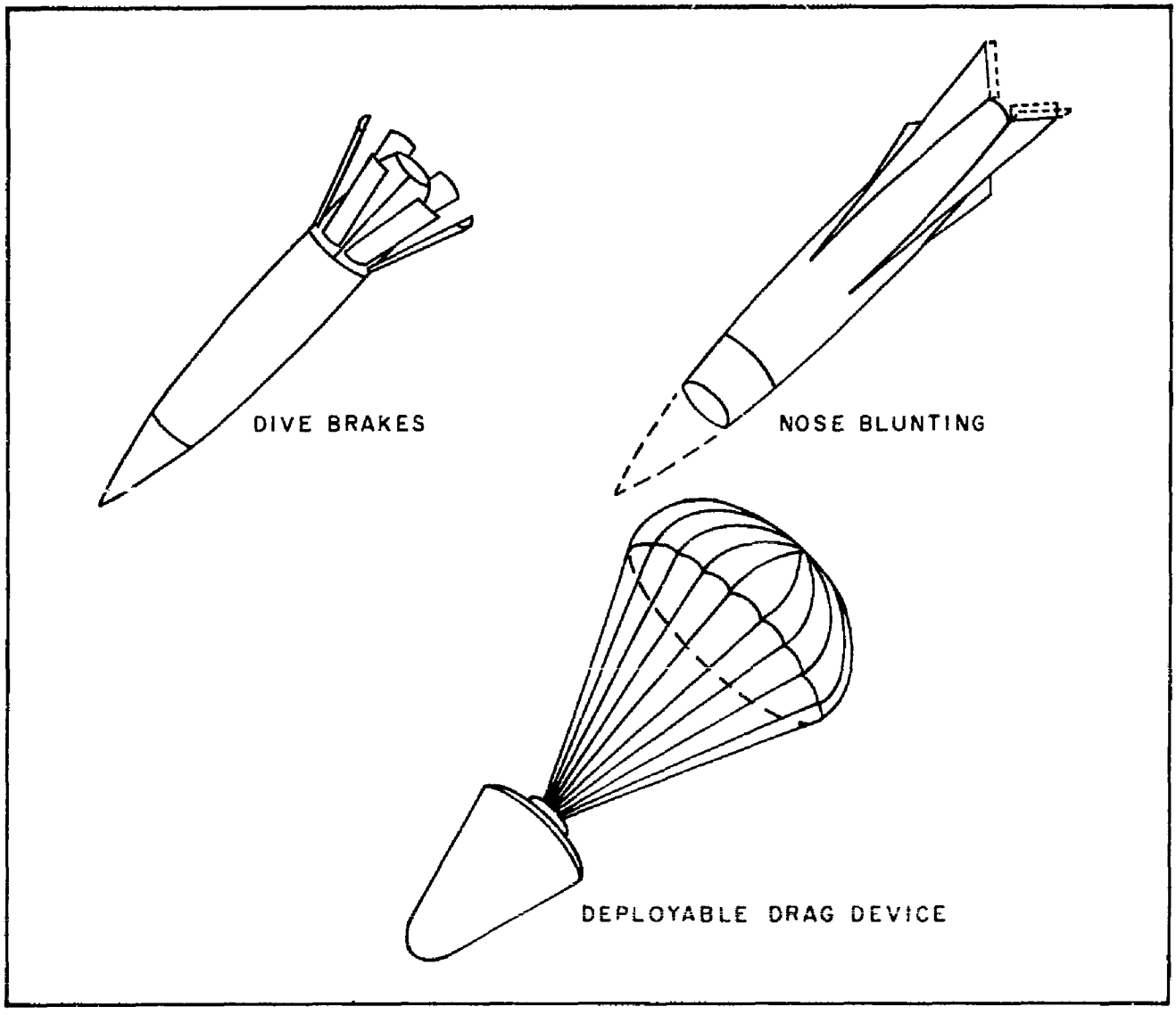

Figure 3. Types of Aerodynamic Deceleration Devices

DEPLOYABLE AERODYNAMIC DECELERATORS

The most efficient and effective means devised so far for augmenting aerodynamic drag, particularly if they can operate outside the turbulent wake of the vehicle, are the deployable aerodynamic drag devices. Examples of the self-inflated and pressure-inflated devices are depicted in Figure 4. The self-inflating device is considered most suitable in the supersonic-speed and relatively high-dynamic-pressure regime of the flight spectrum. This type requires the least weight and, in most cases, the least bulk for a given drag area and is relatively simple in design and operation. This report, therefore, will discuss the self-inflating deployable drag devices and the problems encountered with their operation at supersonic speeds.

At supersonic speeds and relatively high dynamic pressures, the self-inflating aerodynamic deceleration device operates only under "infinite mass" conditions; i.e., the velocity decay of the vehicle-decelerator system during deployment and opening of the deceleration device is extremely small and can be neglected.

Two of the most common types of trailing self-inflating aerodynamic decelerators are the Guide Surface and Ribbon parachute canopies. These parachute canopies have been employed extensively in the initial deceleration of flight vehicles along recovery trajectories. They both have been successfully deployed at transonic velocities, and one type at supersonic velocity.

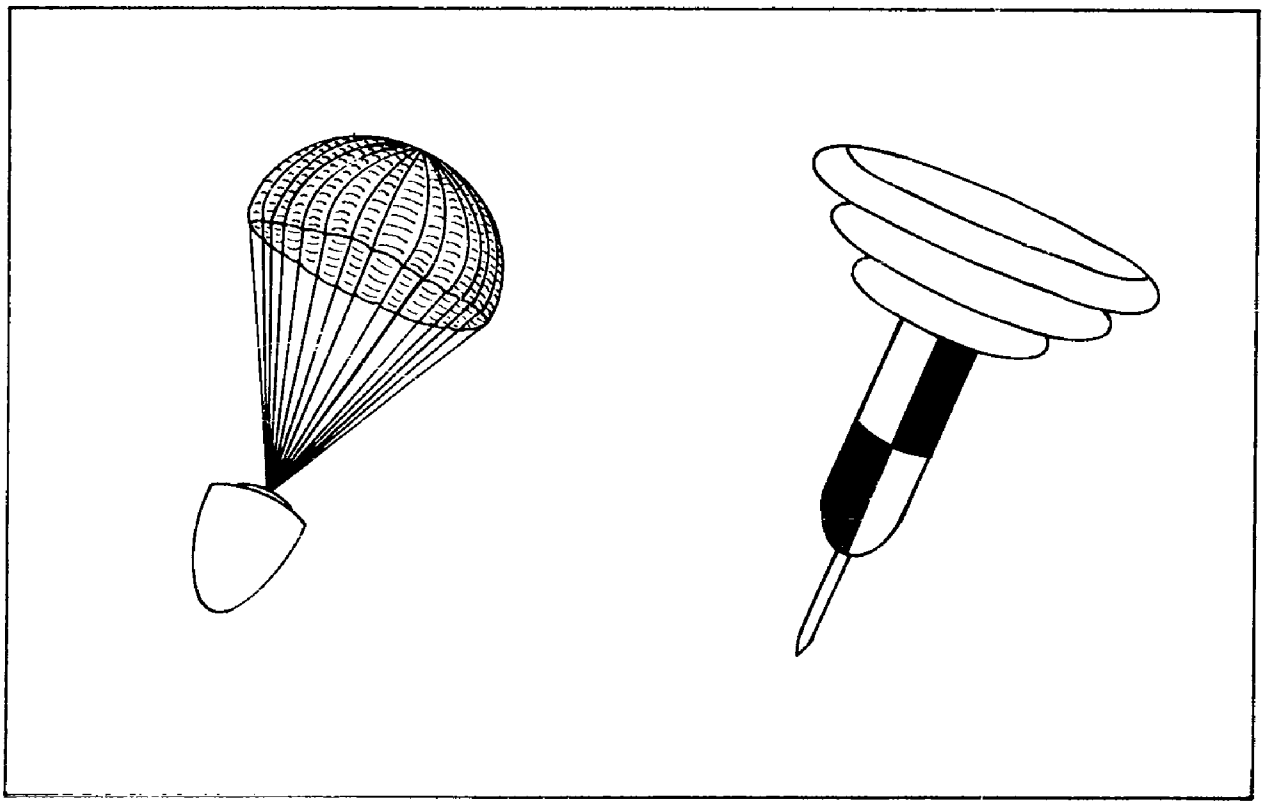

Figure 4. Two Types of Deployable Aerodynamic Deceleration Devices

The Guide Surface type parachute canopy is shown deployed behind a parachute sled test vehicle in Figure 5. The bell-shaped roof panels and guide-surface panels are joined together to form the main seams. In this type canopy, the separation line between roof and conical surface can be considered as a flow-separation edge that creates an effect, as far as stability is concerned, that is identical to that obtained in high-geometric-porosity type canopies. Canopy filling times are very short with attendant opening shock that is relatively high. This effect can be attributed to the low permeability of the cloth used in construction and to the shape of the inflated canopy.

The conventional flat circular ribbon-type parachute canopy is shown deployed behind a sled test vehicle in Figure 6. This parachute is designed with concentric ribbons that are interconnected by a number of radial ribbons and supporting semiradial tapes. Opening and stability characteristics are, to a large extent, a function of total canopy porosity. The porosity must be selected carefully to assure desired canopy performance.

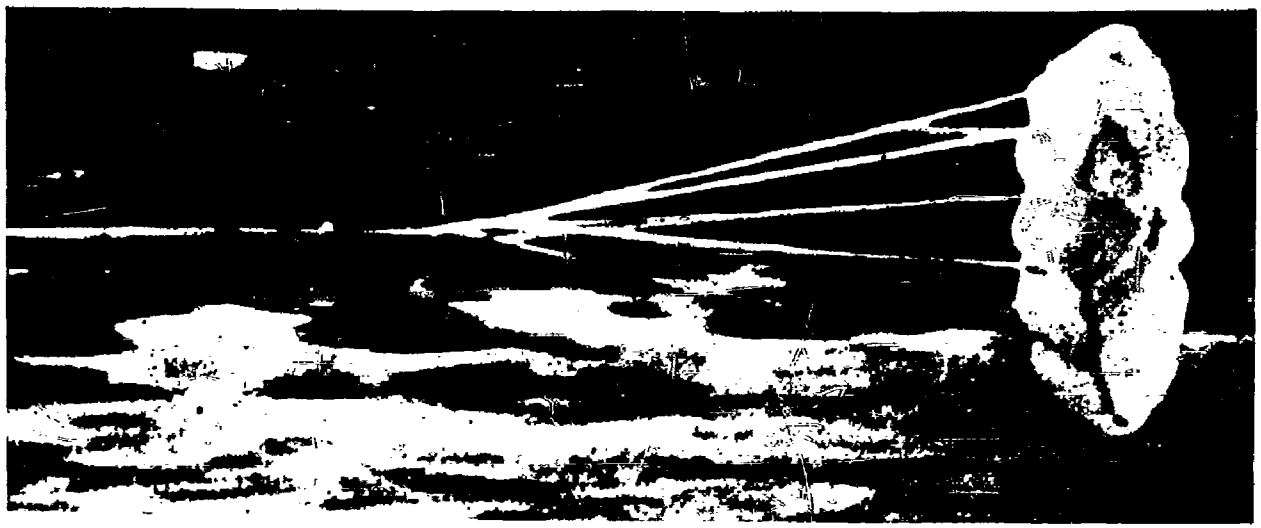

Figure 5. Guide Surface Type Parachute Canopy

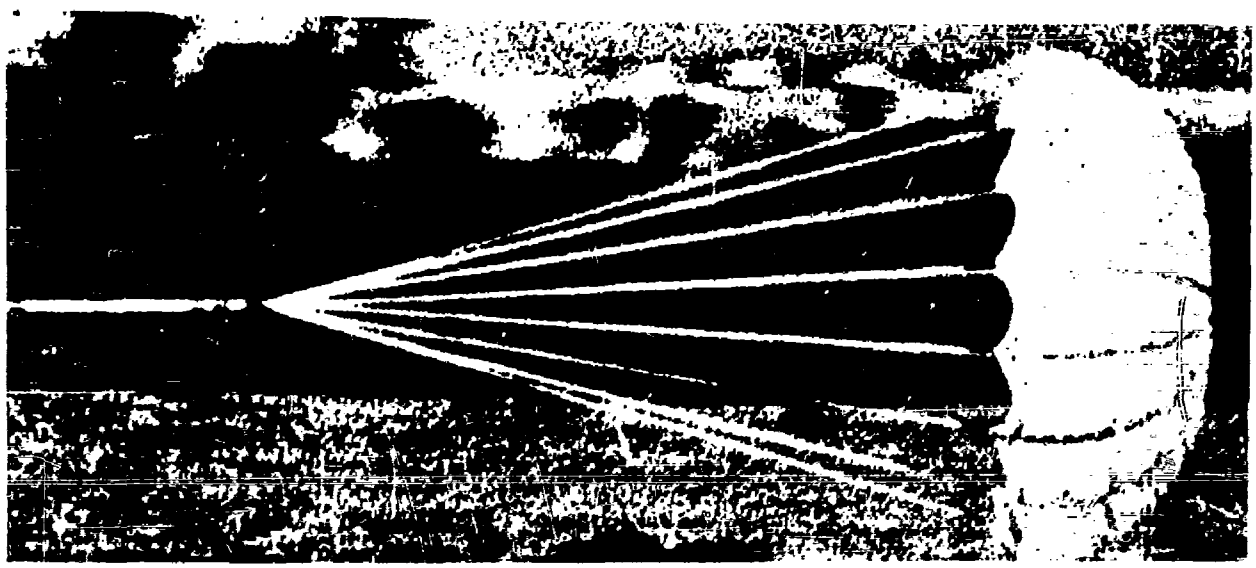

Figure 6. Flat, Circular, Ribbon-Type Parachute Canopy

PARACHUTE CANOPY OPERATION IN THE TRANSONIC SPEED REGIME

Considerable design and performance data for Guide Surface and flat circular ribbon-type parachute canopies operating in the high subsonic and transonic speed ranges is available. This data was obtained, primarily, from a test program using rocket-propelled-sled test vehicles. The test parachute canopies were deployed behind the sled at desired speeds and the aerodynamic and general performance characteristics were measured and recorded. Parachute canopies tested had a subsonic drag area, $(C_DS)_{o,p,}$ of between 16 and 28 square feet. A drag area of 28 square feet was chosen as the upper limit because this area will, in all probability, be the largest drag area employed for initial deceleration in recovering vehicles from flights at supersonic speed and high dynamic pressure.

Comparative performance characteristics for the two parachute canopy types are shown in Figure 7 (Ref. 1). The data plotted represent the total drag force generated and transmitted to the vehicle, the ratio of inflated (projected) canopy area to design (nominal) canopy area, and the oscillatory motions of each of the parachute canopies during the test run. All data are plotted versus a common time scale; a second scale for sled speed is added for comparison. In addition, parachute canopy drag coefficients, $C_{D_{o,p,}}$ are plotted versus Mach number. Near normal performance characteristics were recorded and drag coefficients were only slightly reduced during the higher speed portions (above Mach 0.95) of individual test runs. In interpreting these and other parachute performance data, the drag coefficient, C_{D_p}, for the Guide Surface type parachute canopies is based on the theoretical projected area, S_p, which in this case is equivalent to the area defined by the constructed canopy diameter, D_c. For all other types of parachute canopies, the drag coefficient, C_{D_o}, is based on the total canopy cloth area, S_o, or the nominal parachute canopy area.

Figure 8 shows the relationship of the ratio of opening force, F_o, and nominal area of the parachute canopy, S_o, to the dynamic pressure, q_c, at snatch force. Both types of parachute canopies are operating under essentially infinite mass (canopy drag loading $\frac{W}{C_DS}$ = 125 lb/ft^2) and near sea-level density conditions. The curve for the Ribless Guide Surface type parachute canopy shows an essentially linear increase in opening force with dynamic pressure up to a dynamic pressure of 1500 lb/ft^2 and an equivalent Mach number of 1.08. The curve up to that point follows a theoretical curve derived by considering the value of the opening shock or X factor to be 1.40. This relationship indicates consistent and full inflation of the Ribless Guide Surface type parachute canopy; however, an increase in dynamic pressure or Mach number results in a flattening of the curve. The curve for the flat, circular, ribbon-type parachute canopy shows a more pronounced flattening with increasing dynamic pressure, indicating longer filling times and a tendency toward reduced canopy inflation. The theoretical relationship was derived by considering an opening shock or X factor of 1.05. Motion pictures taken during these tests substantiated the assumption that initial canopy squidding caused reduced drag generation: in the Guide Surface type parachute canopy, the guide surfaces are partially inverted at the higher velocities and become normally inflated as the velocity decays. The ribbon-type parachute canopy initially exhibits a reduced projected diameter at the

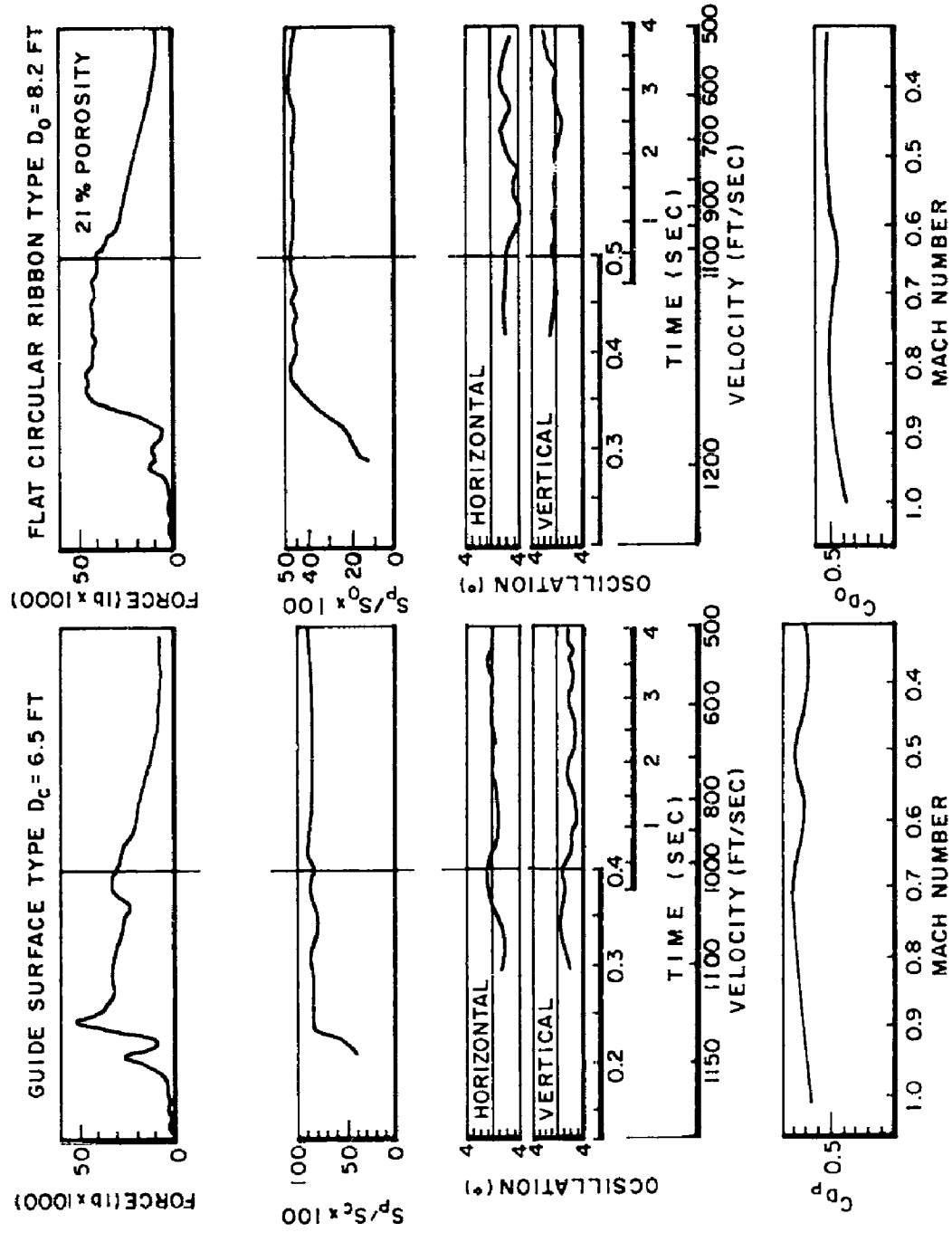

Figure 7. Comparative Performance Characteristics of Two Parachute Canopies at Transonic Velocities

higher velocities and becomes fully inflated after velocity is reduced to subsonic. Primary body wake effects did not cause this somewhat abnormal behavior at the higher operational velocities since the canopies were at a distance of more than 12 primary-body diameters behind the vehicle, and the ratio of inflated canopy diameter to primary-body diameter was, in all cases, larger than 6. At first, the abnormal canopy performance was believed to be caused by high dynamic pressures; it was established later, however, that the causes are primarily Mach number effects.

All Guide Surface type parachute canopies were extensively damaged when they were deployed at dynamic pressures greater than 1700 lb/ft^2. Neither materials nor seams and stitching patterns have been developed that promise to extend the operational capabilities of this type canopy beyond this dynamic pressure limit. On the other hand, no significant strength problem has become evident to prevent the use of ribbon-type parachute canopies at the higher dynamic pressures. Therefore, efforts to extend the operational capabilities of parachute canopies into the supersonic high-dynamic-pressure flight regime are emphasizing the ribbon-type parachute canopy.

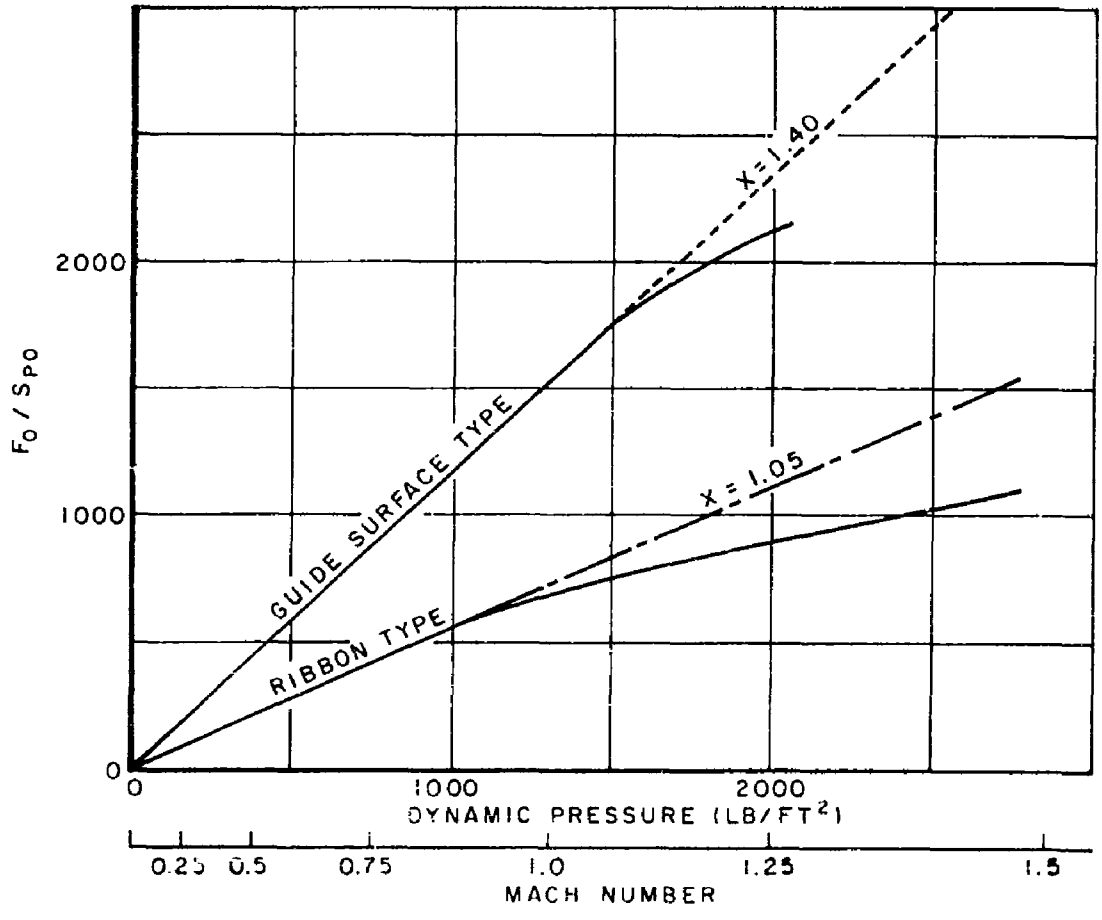

Figure 8. Ratio of Opening Force to Canopy Area Versus Dynamic Pressure and Mach Number for Guide Surface and Flat, Circular, Ribbon-Type Parachute Canopies

PARACHUTE CANOPY OPERATION IN THE SUPERSONIC SPEED RANGE

Erratic canopy opening and performance characteristics at operational speeds above Mach 1 were observed in sled tests in the transonic speed range. A severe problem was also evident during wind-tunnel and free-flight tests at Mach numbers up to 3.5 (Refs. 2 and 3). In these tests, both the flat, circular, ribbon-type and Guide Surface type parachute canopies exhibited erratic inflation tendencies, violent canopy pulsing or breathing, considerably reduced drag, and failure of cloth, ribbons, and suspension lines at a fraction of their rated strengths. A film sequence is shown in Figure 9 illustrating the typical breathing or pulsation cycles of two flat, circular, ribbon-type parachute canopies having total canopy porosities of 29.4 and 5.6.

Failure was the result of fatigue caused by flutter of the material at the low load conditions that prevailed throughout the tests. Inflation of the flat, circular, ribbon-type parachutes was never greater than about 70 percent, and was as low as 30 percent of maximum canopy diameter at subsonic velocities. As a result, drag-producing capabilities were reduced to values that ranged from 80 percent of theoretical at Mach 2.0 to 33 percent at Mach 3.5.

The geometric porosity of the ribbon-type parachute canopies was varied from 5 to 30 percent. In addition, the porosity distribution was varied by holding the skirt porosity low and vent porosity high, and vice versa. Horizontal and vertical ribbon spacings also were varied. These variations in canopy design neither changed nor improved canopy performance significantly.

Guide Surface type parachute canopies exhibited reduced inflation characteristics and severe flutter in all cases of supersonic operation. The guide surface portions were indented inward and the canopy top was over-extended. The material burst immediately at the juncture of the two sections.

A number of investigations and analyses were conducted to determine the causes for this abnormal canopy operation and establish a basis for designing more suitable canopies for supersonic operations. A test program was conducted using flexible and rigid models of drag-producing surfaces and parachute canopies to determine flow and pressure distribution. These tests are described as follows.

Drag-Producing Surface, Rigid Model Tests

Tests were conducted on the drag-producing surface of a flat, circular, ribbon-type parachute canopy having a geometric porosity of 20 percent at Mach 1.7 to 3.5. Results of these tests indicated that, in most cases, the flow through the drag-producing surface was choked, as shown in Figure 10, much like the flow in a ramjet inlet diffuser in subcritical operation. The flow at the entrance of the drag-producing surface and everywhere inside the model is subsonic because a detached shock wave is present in front of the drag-producing surface. Actually, the tests show that two shock regimes could exist: one, the usual or normal shock configuration, can exist throughout the range of Mach numbers and Reynolds numbers; this shock configuration can change to the unusual form shown in Figure 11 at identical conditions and for reasons as yet unexplained. Either shock configuration exists in a very steady stable sense, but the configuration shifts from one to the other very abruptly and without correlation to Mach number or Reynolds number. In some instances, the change requires several seconds, and in others, several minutes.

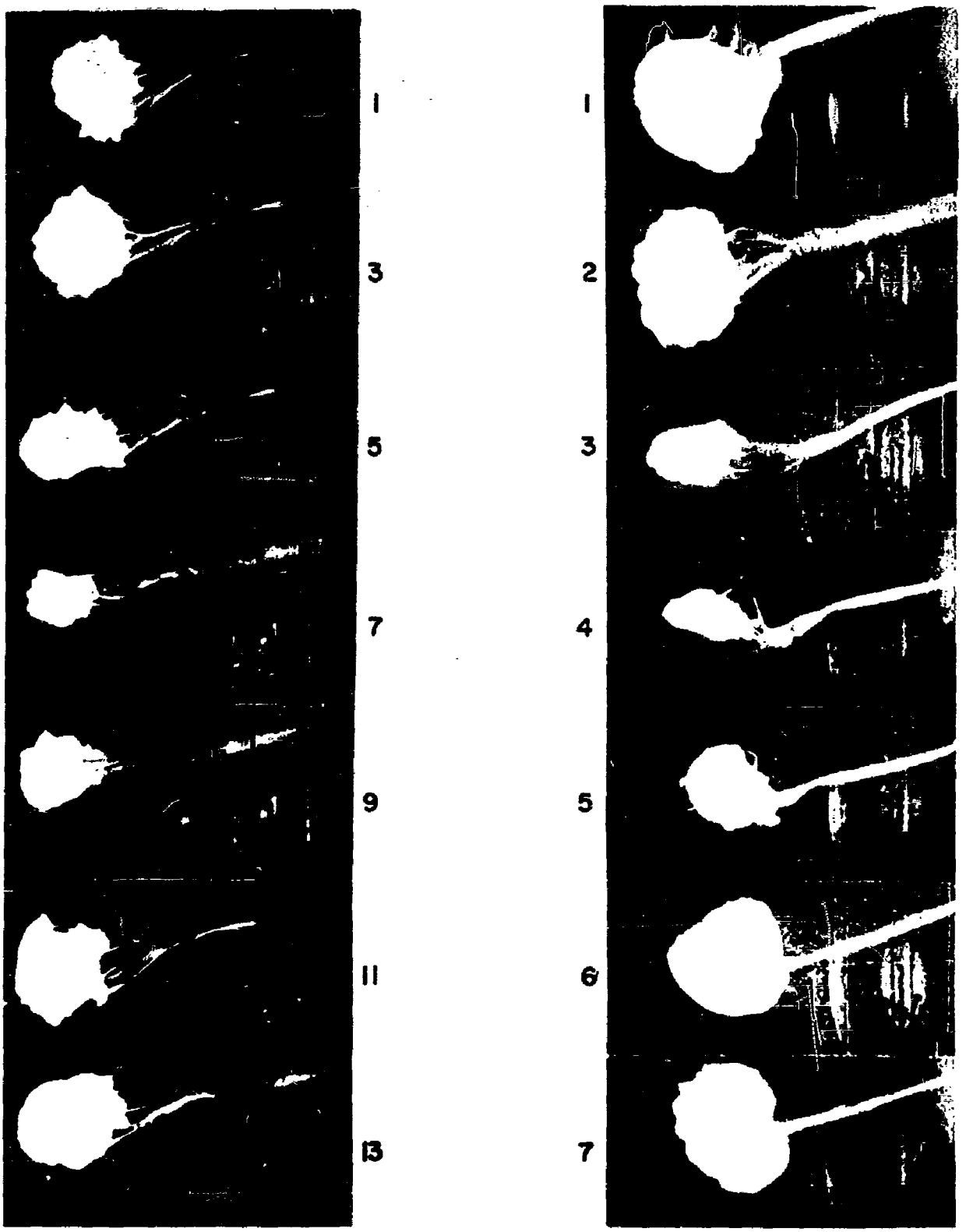

Figure 9. Flat Circular Ribbon-Type Canopy Operation at Supersonic Speeds (Mach 3.5)

Figure 10. Ribbon-Type Drag Producing Surface, Usual Shock-Wave Formation

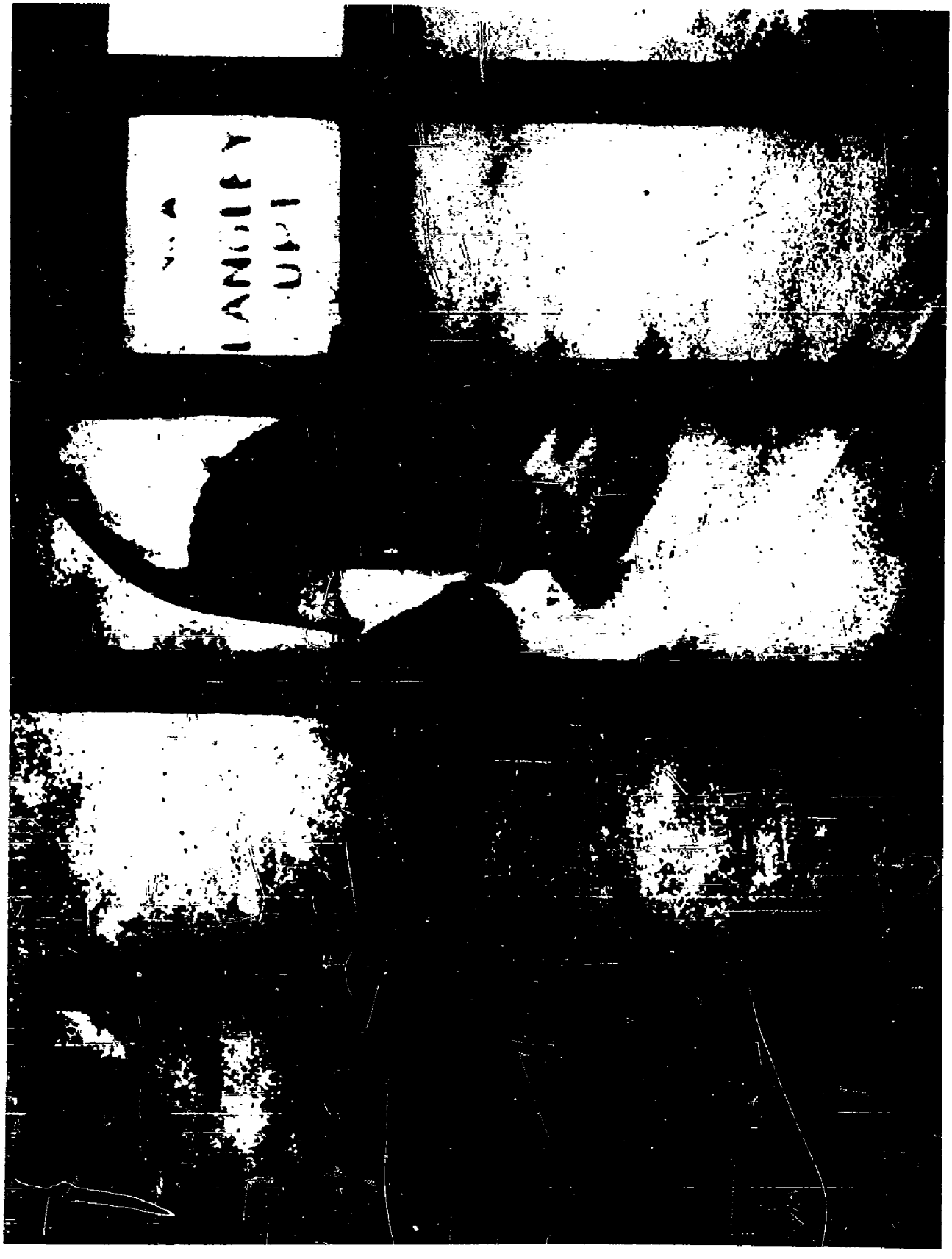

Figure 11. Ribbon-Type Drag Producing Surface, Unusual Shock-Wave Formation

Fredette (Ref. 4) analyzed this shock-wave peculiarity by first plotting the shock wave standoff distance versus Mach number, and then superimposing this plot on the unusual form of the shock profile existing in Figure 11. Shock-wave standoff distance versus Mach number for various ratios of exit (porosity) area to intake (mouth opening) area is plotted in Figure 12. The zero porosity case represents a flat circular disk positioned normal to the airflow. The curve for 20 percent porosity was obtained by assuming that the percentage of airflow escaping through the openings of the drag-producing surface would proportionately reduce the spill-over at the skirt as well as the distance from the shock wave to the edge of the drag-producing surface without substantially altering the shape of the shock wave. With these simple assumptions, correlation of data and estimates is surprisingly good.

A superposition of this information on a sketch of the unusual form of shock profile for the drag-producing surface is shown in Figure 13, together with the airflow lines that probably exist inside the drag-producing surface. The standoff distance of the bulged portion of the shock wave is roughly equivalent to that which would be expected for a zero-porosity disk. The standoff distance for the remaining portion of the shock wave is equivalent to that associated with the porosity of the drag-producing surface. The idealized streamlines shown are only speculations associated with the shock wave form. No detailed calculation of the internal flow has been attempted; however, this unusual shock-wave form may be generated by very small disturbances that are propagated asymmetrically and are due to model changes or vibrations and fluctuations in the airstream. In the case of a solid cup, an increase in spill-over airflow on one side would have to be accompanied by a reduction on the other side. In the case of a porous cup, however, high internal velocities tangential to the surface of the cup may greatly reduce the mass flow out of the slots on the bulge side of the shock wave. That portion of the drag-producing surface, therefore, would be effectively imporous and sustain the unsymmetrical shock form. The shock-wave standoff distances shown in Figure 13 indicate indirectly that the effective porosity is zero in one portion of the drag-producing surface and normal in the remaining portions.

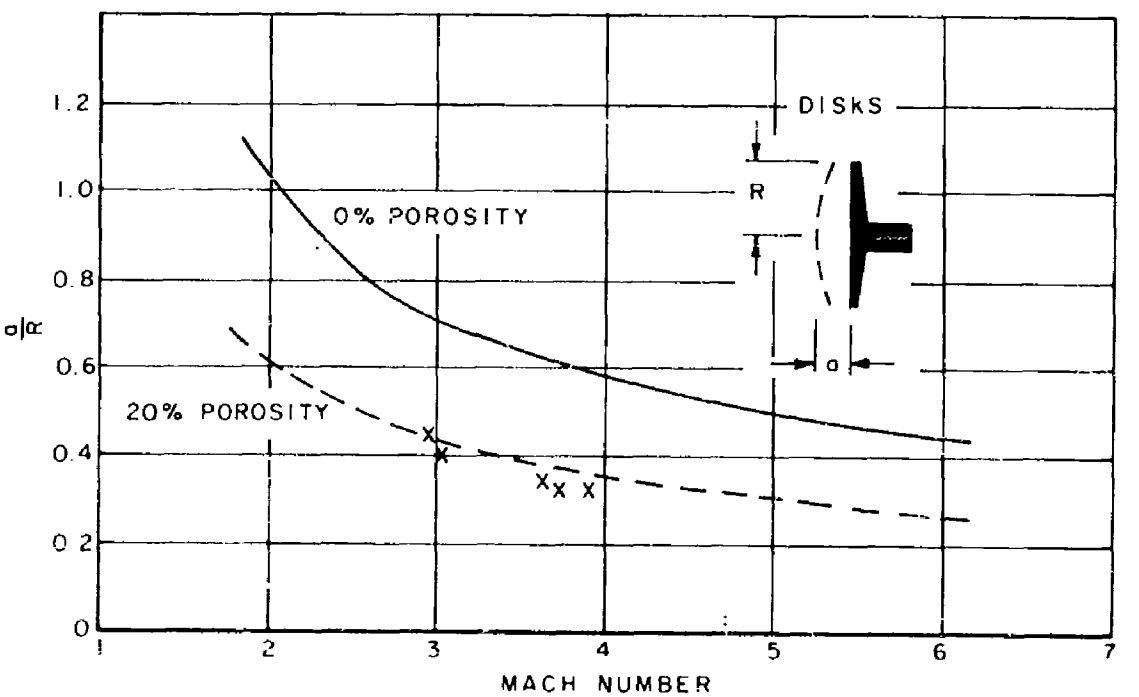

Figure 12. Ratio of Shock Wave Standoff Distance to Blunt-Body Radius Versus Mach Number

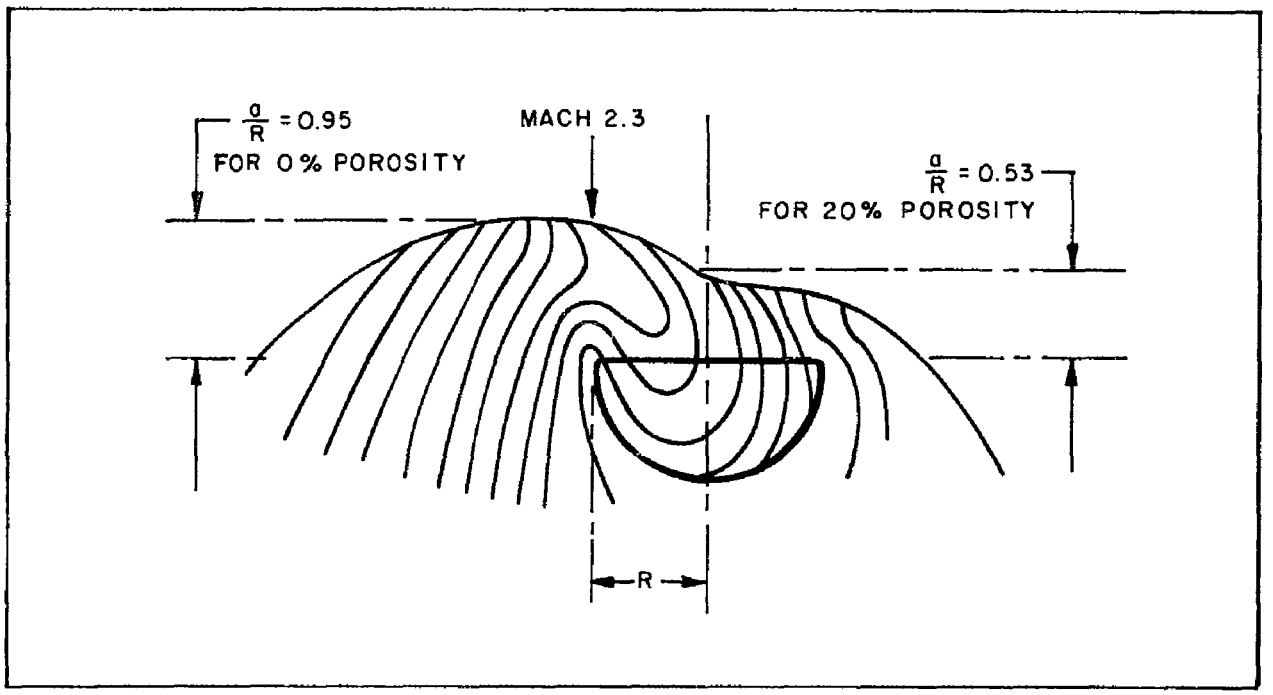

Figure 13. Shock-Wave Pattern at Mach 2.3

Naturally, unsymmetrical shock-wave configurations must be avoided in flexible parachute canopies since they would create asymmetric internal pressure distributions. These asymmetries could distort the drag-producing surface and excite fluctuations. On the basis of rigid model tests, asymmetrical shock forms and choked flow can be avoided by incorporating either higher porosities or a large vent.

Canopy porosity or the ratio of outflow area to inflow area required to achieve air-flow conditions yielding zero air spill-over around the skirt of the drag-producing surface can be calculated. Assume that the flow in the slots between adjacent ribbons has sonic velocity and equate the air mass flows in free stream, behind the normal shock, and in the slots of the drag-producing surface. This required porosity, when incorporated into a rigid drag-producing surface, produced stable shock patterns in the wind tunnel. Reducing the free-stream Mach number, however, again resulted in choked flow and unsteadiness of the flow field.

Drag-Producing Surface, Flexible Model Tests

The analysis of test results on rigid models of the drag-producing surface indicated that the internal flow characteristics of the drag-producing surface cause most of the unsteadiness of the flow field and erratic behavior of the flexible parachute canopies. Since three-dimensional models do not allow observations of the flow within the inflated drag-producing surface, Heinrich (Ref. 5) performed tests on two-dimensional models of flexible solid-cloth-type and ribbon-type drag-producing surfaces. These experiments were conducted at a velocity equivalent to Mach 2. The principles of water-surface wave analogy were employed, in which a flexible model is towed in shallow water and the wave formations are recorded photographically. Giving due consideration to the differences between flow in water and flow in air, we can see that model behavior in water and in wind tunnels are similar.

An analysis of recordings on two-dimensional parachute canopy models without suspension lines shows the same variety of flow patterns for wide open and closed parachute canopies as was observed during wind-tunnel tests. Random motions of fluid particles observed in water were significantly similar to those observed or suspected in air, such as fluid particles spilling to one side, the mass of fluid being expelled from the inside of the canopy into the surroundings, reflection of pressure waves, and others.

The drag-producing surface is filled when a pressure area develops inside the cup. At the beginning, this pressure area is evenly distributed, as indicated in Figure 14, which represents wave formations obtained during the water tow tests. This pressure area forms a fairly even high plateau that changes abruptly across or slightly upstream from the skirt of the drag-producing surface. This normal pressure ridge recedes with time. As a consequence, a small high-pressure area is developed in the apex area of the drag-producing surface. Since the pressure in the skirt then becomes considerably lower than that in the apex area, the skirt area contracts and reduces the inlet diameter. The pressure near the skirt of the drag-producing surface is then lower than that of the surrounding flow, so particles move toward the drag-producing surface. This condition is often accompanied by a pronounced pressure ridge moving inwardly. This moving pressure ridge may be met by a pressure ridge reflected from the apex toward the skirt. These inward and outward moving waves generally collide, interfere with each other, and create an infinite variety of ridge and valley formations in and about the drag-producing surface. The pressure ridges moving inside the drag-producing surface change the shape of the flexible model continuously from nearly hemispherical to elongated.

This water analogy study showed that whenever the interior of the flexible drag-producing surface is filled with a fairly uniform high-pressure plateau, the inlet diameter is relatively large. A well-developed high-pressure area is usually accompanied by a main bow wave slightly upstream of the inlet area. Pressure plateaus in the apex of the drag-producing surface, however, usually produce a small inlet area and an elongated shape.

Drag-Producing Surface, Pressure Distribution

Heinrich, Ballinger, and Ryan (Ref. 6) studied the pressure distribution over the drag-producing surface of a rigid parachute canopy of the flat, circular, ribbon-type at transonic Mach numbers, assuming that the inflated drag-producing surface is of hemispherical shape. Suspension lines were not included. Pressure taps were located along center lines of opposite gores of the model.

Internal and external pressure coefficients, c_p, were determined for a range of Mach numbers. The coefficient of pressure was defined by:

$$c_p = \frac{\text{Local Static Pressure - Free Stream Static Pressure}}{\text{Dynamic Pressure}} = \frac{\Delta P}{q}$$

The variation of external pressure coefficient with Mach number at the pressure taps on the drag-producing surface is plotted in Figure 15. In general, the negative values for external pressure coefficient decrease with increasing Mach number. Values for internal pressure coefficient, in all cases, approximate the ratio $\frac{\Delta P}{q}$ of compressible flow and increase with free-stream velocity. The net change in the pressure distribution, however, represents a decrease in the self-inflation of a flexible drag-producing surface.

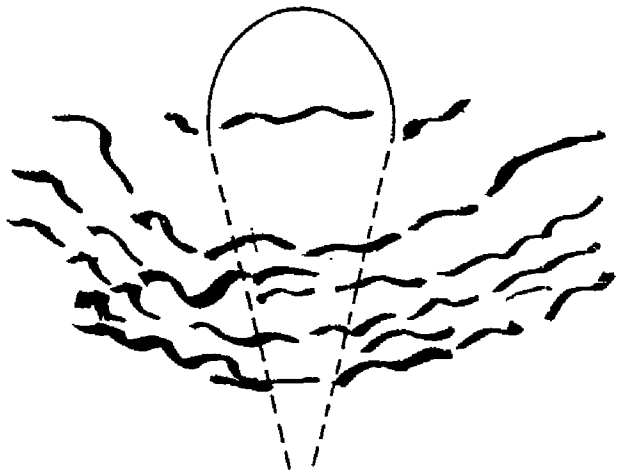

a. Forward Ridge at Mouth of Canopy, Canopy Open Diameter Enlarging

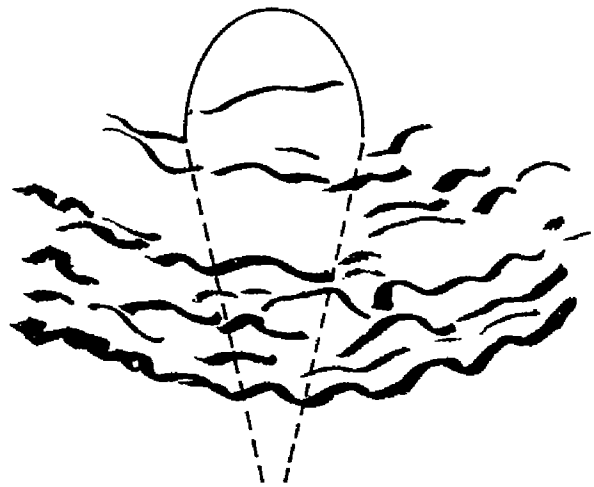

b. Forward Ridge Beginning to Dissipate

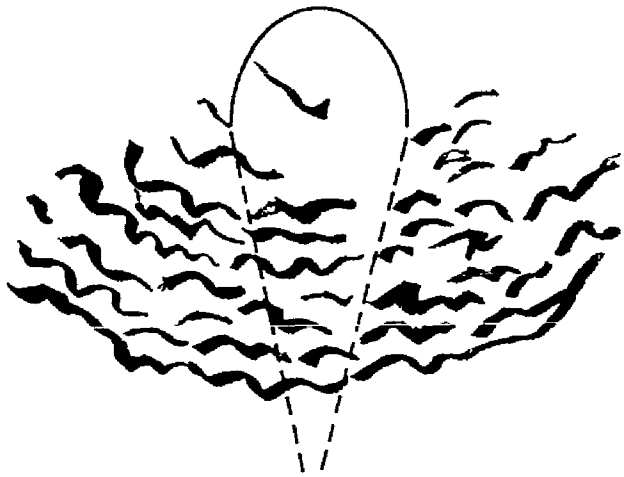

c. Forward Ridge Dissapated; Flow Beginning to Enter Canopy

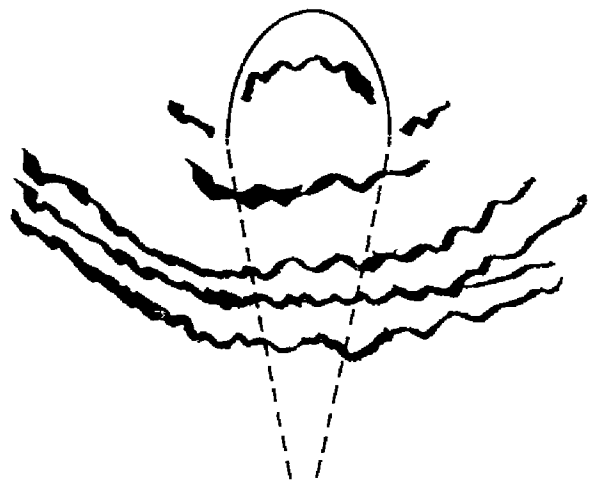

d. Pressure Ridge Starting to Move Forward; Canopy Open Diameter Near Minimum

Figure 14. Sequence Showing Correlation Between Shock Patterns and Pumping for a Flexible, Solid, Flat, Parachute Model at a Simulated Speed of Mach 2.2

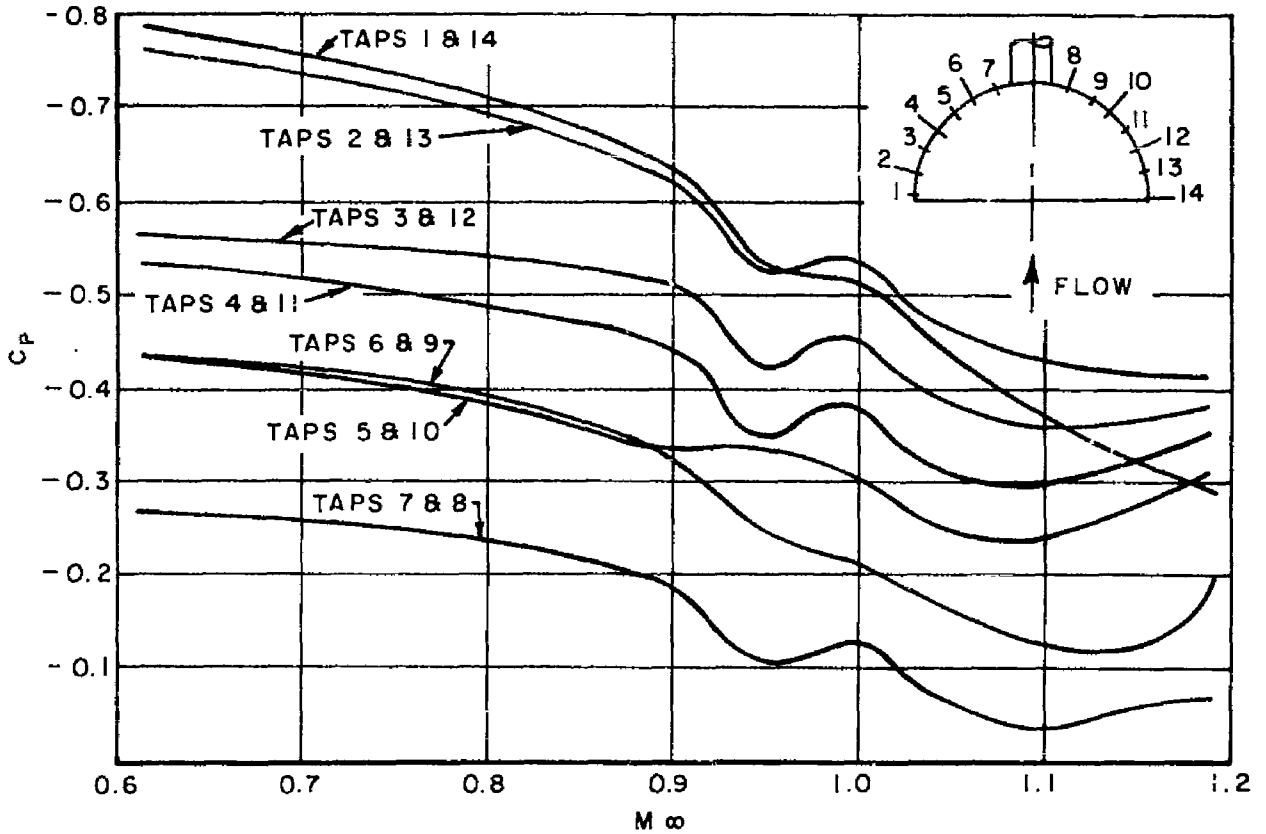

Figure 15. Pressure Coefficient, c_p, Versus Free-Stream Mach Number for Ribbon-Type Drag-Producing Surface

These pressure distributions were measured on a hemispherical body of revolution; scallops that normally form on inflated parachute canopies in operation were not simulated. In addition, suspension lines were omitted, and these lines, as will be shown later, have a significant effect, particularly upon the internal pressure coefficient. Nevertheless, these simple pressure-distribution measurements indicated an inflation problem for the ribbon-type parachute canopy in supersonic flow.

Parachute Canopy, Rigid Model Tests

Wind tunnel tests of rigid models of parachute canopies were conducted (Ref. 7) to study the shock-wave and flow pattern ahead of and around the canopy model and the effects of suspension lines on canopy behavior. Canopies with drag-producing surfaces having geometric porosities of 20 and 45 percent were utilized. These porosities were obtained, primarily, by incorporating a large vent. The canopy of 45 percent porosity was tested with 24, 12, and 6 suspension lines of 1 D_o length at Mach 1.5 to 2.76. The canopy of 20 percent porosity was tested with 24 suspension lines of 1 D_o at the same Mach number range. Typical shock-wave formations recorded during these tests are shown in Figure 16. The flow characteristics of these configurations were essentially the same.

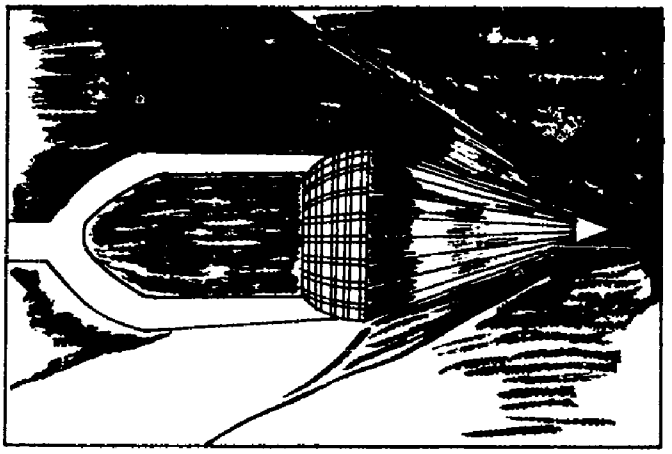

45% (Large Vent) Porosity Ribbon Type Canopy, M = 2.76

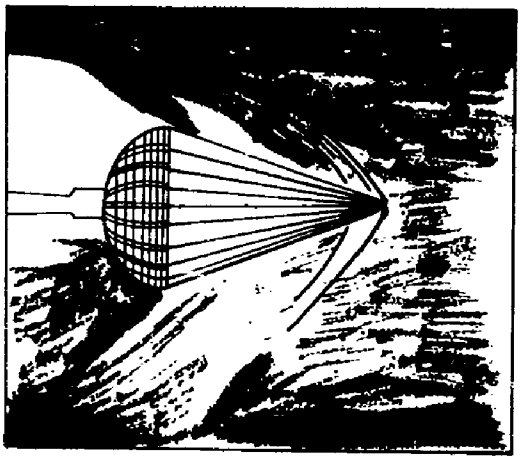

20% Porosity Ribbon Type Canopy, M = 1.57

Figure 16. Typical Shock Wave Formations

Additional tests were conducted on both types of parachute canopies with 24 suspension lines of 2 D_o length. At Mach 3.71, the 20-percent-porosity canopy formed flow patterns similar to those observed with 1 D_o lines; the 45-percent-porosity canopy, however, formed an entirely different flow field at Mach 2.98. In this case, a conical shock wave, terminating in a normal shock wave on the centerline of the configuration, existed inside the suspension lines. This conical shock wave fluctuated slightly in the axial direction between the limits shown in views a and b of Figure 17. In the view shown in Figure 17a, normal shock waves are seen emanating from the skirt of the canopy; these waves do not exist in view b. We conclude that the flow field is subsonic at the skirt of the canopy in view b, but supersonic in view a.

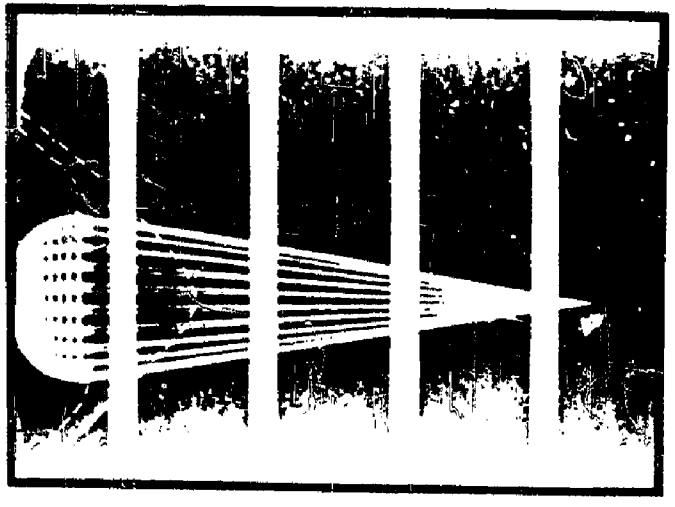

a. M = 2.98

c. M = 3.71

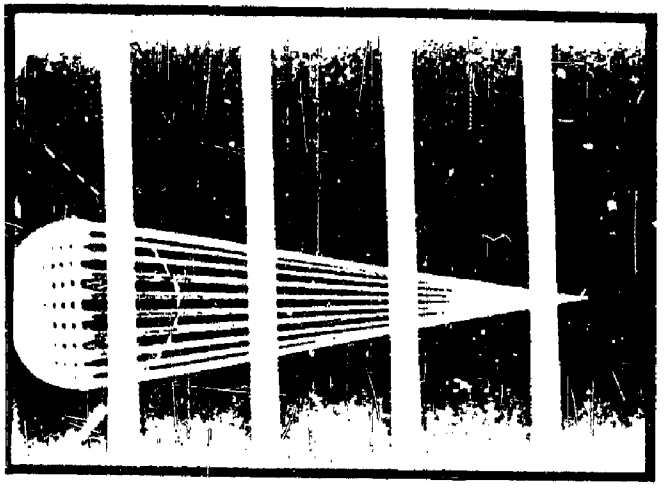

b. M = 2.98

d. M = 3.71

Shock waves traced from original negative in portions where reproductions are poor.

Figure 17. Shock Waves for 20% Porosity Canopy with 2.0 D_o Suspension Lines at Two Mach Numbers

With suspension lines of 1 D_o length, we observed no differences in the flow characteristics with variation of number of suspension lines, canopy porosity, or Mach number. With suspension lines of 2 D_o, however, flow characteristics differed substantially with Mach number. Fredette's analysis (Ref. 4) indicates that this difference must be due to the wake generated by the cone extension formed by the suspension lines at the forward end of the model and by blockage of airflow by the lines as they converge at the base of the cone. Since the suspension lines, themselves, appeared to affect flow behavior very little, Fredette assumed that the wake created by the blockage of airflow by the conical extension is the predominant effect. Velocity on the wake centerline at the canopy skirt is considerably lower with suspension lines of 1 D_o than with lines of 2 D_o. Consequently, the initial interaction of the shock wave emanating from the skirt with this wake profile would be quite different for the two configurations. Fredette further analyzed the wake behind the conical extension and considered the velocity distribution in the wake. The normal shock was considered as well as the rise in conical shock pressure that determines the stable point for the shock wave inside the suspension lines. No point of stable equilibrium can exist between the base of the conical extension and the drag-producing surface if shorter line lengths are used so that the Mach number on the core of the wake is lower or if longer line lengths are used but the free-stream Mach number is higher so that a given conical shock angle can attain and sustain higher pressures. In this case, the canopy shock will move forward to combine with the conical shock from the cone extension. The wake from the conical extension will not close and the entire region inside the suspension lines will be in a subsonic turbulent wake condition at a pressure level approximating that behind the cone extension.

Parachute Canopy, Flexible Model Tests

Additional tests were conducted on fabric canopy models (Ref. 8) to supplement the data from tests of the rigid models. A forebody of only minimal diameter was employed. The shock wave and flow properties were essentially identical to those seen in tests of rigid models. When a forebody having a frontal area approximating that of a normally fully inflated canopy was used, a rather rounded shock wave formed ahead of the canopy, as shown in Figure 18. These tests showed that the shock wave interacts with the suspension lines only when the shock plane is perpendicular to the lines or when the edge of the canopy approaches the shock wave itself. Canopies of higher porosity (40 percent) inflated less than canopies of lower poroisties, and their oscillation relative to the attachment point was considerably less. This observation is compatible with results indicating that porosity affects the canopy stability relative to the point of suspension.

Canopies positioned behind a forebody of relatively large diameter behave better because of the favorable effects of the body wake characteristics. The favorable effect of an upstream body was further substantiated in tests of an extended-skirt ribbon-type parachute canopy (Equiflo canopy) of 28 percent porosity with an inflated tube attached to the skirt. When the tube was added, the canopy became very stable and a stable, curved shock wave was generated ahead of the canopy, as shown in Figure 19. The flow field in back of this shock wave is obviously subsonic since no shock wave is seen arising from the edge of the tubular skirt. A comparison of the shock waves depicted in Figures 18 and 19 with that at M = 2.98 in Figure 17a shows rather different shock-wave formations. While both Mach number and relative wake size are important in explaining the differences, the relative wake size appears to predominate. The width of the undisturbed wake in Figure 17a is approximately 0.2 of the diameter of the canopy, but is comparable to the canopy diameter in Figures 18 and 19. When the wake width relative to the canopy diameter approaches unity, the region of shock diffraction

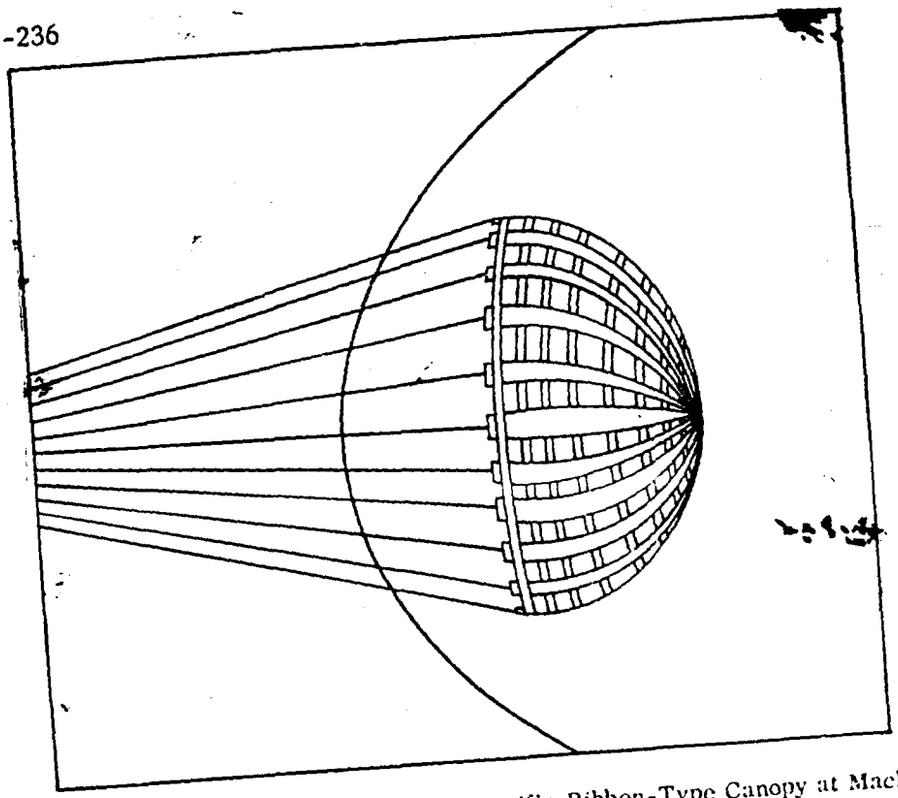

Figure 18. Shock Wave for 28% Porosity Equiflo Ribbon-Type Canopy at Mach 2.2 with 2 D_o Lines at 7 Diameters Behind a Forebody

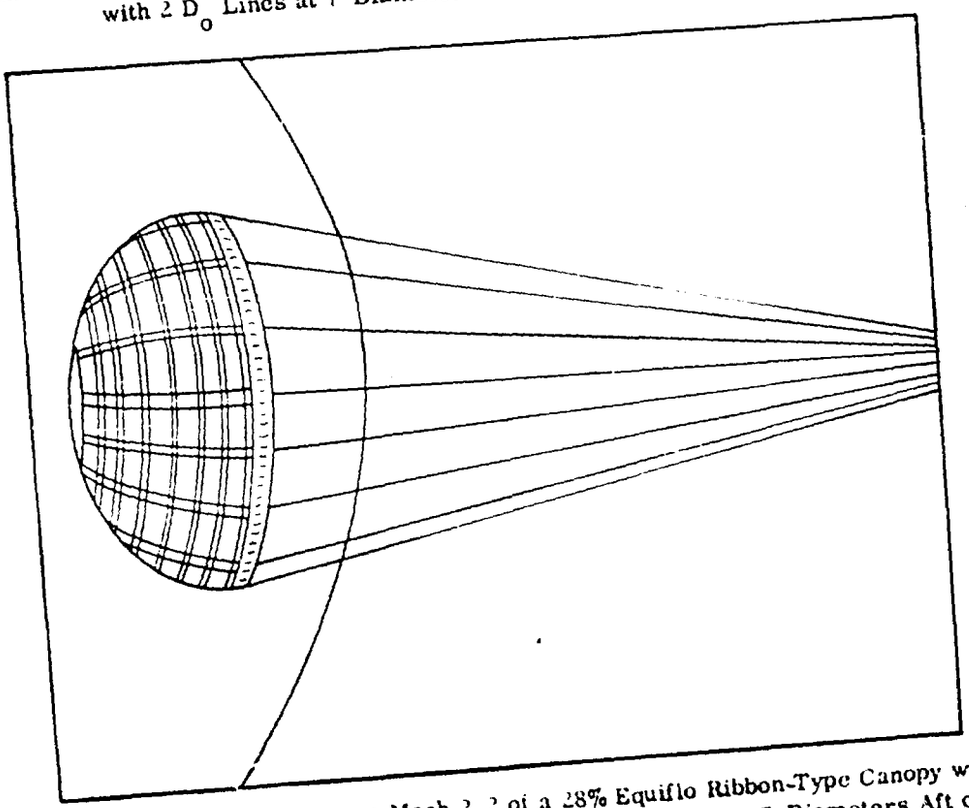

Figure 19. Characteristics at Mach 2.2 of a 28% Equiflo Ribbon-Type Canopy with a 5% Thick Inflated Torus Attached to the Skirt at 7 Diameters Aft of the Body

due to velocity shear ahead of the shock wave extends over the entire region of the canopy and allows the shock wave to clear the skirt lip with subsonic spill-over, without requiring separation of the wake itself. This is the condition depicted in Figure 17, views c and d. Consequently, the relative size of the wake, if large enough, has a very favorable effect. The effect of the wake structure shown in Figure 17c and d has not been evaluated in actual tests of fabric canopies; however, as was observed in earlier tests, canopy breathing may be anticipated because fluctuation is inherent in such separated flows.

Parachute Canopy Pressure Distribution

An analysis of the external and internal pressure distribution on a ribbon-type parachute canopy in supersonic flow was continued by Heinrich (Ref. 5). The primary objective of these tests was to determine the effects that suspension lines and the location of a primary body of revolution upstream from the canopy have upon the canopy pressure distribution.

The parachute canopy was of the flat, circular, ribbon type with a geometric porosity of 26 percent, evenly distributed. The inflated shape of the canopy was the flying shape, as determined by photographs taken of a model textile canopy in subsonic flow. The projected diameter of the pressure distribution models was 1.94 inches. Ten pressure taps were located along centerlines of opposite gores of the model so that effects at any angle of attack could be evaluated. The taps were positioned on alternate ribbons beginning with the skirt ribbon. The primary body of revolution was a 1.94-inch-diameter, 2.5-caliber, ogive cylinder with a fineness ratio of 4.5.

The first series of pressure distribution measurements was conducted on a drag-producing surface with and without lines in free stream at transonic Mach numbers and Mach 3. The external and internal pressure coefficients versus Mach number recorded at the various tap positions are shown in Figure 20. External c_p values are slightly different from those shown in Figure 15. This difference in values must be due, primarily, to the difference in model shapes. The internal pressure distribution for the model without lines was nearly constant, and the values of the pressure coefficients were approximately equal to the ratio of $\frac{\Delta P}{q}$ of compressible flow. Internal c_p for the model with lines changed, particularly at the higher Mach numbers.

The second series of measurements was made on a drag-producing surface with suspension lines and a forebody positioned at a distance of eight forebody diameters upstream. The external and internal pressure coefficients for the Mach number range investigated are shown in Figure 21. By comparing Figures 20 and 21, we can see that the influence of the forebody is small on both internal and external pressure coefficients. Figure 20 shows that suspension lines influence the magnitude of the internal pressure coefficients noticeably, particularly at the higher free-stream Mach numbers. The effect of suspension lines on the external pressure coefficients, however, is relatively small. The internal pressure coefficient for the drag-producing surface without lines is higher due to the large pressure recovery across the well-defined shock wave ahead of the drag-producing surface.

Shaped-Gore Ribbon-Type Parachute Canopy

An extension of the operational capabilities of conventional parachute canopies into the higher supersonic speed regimes, as shown by results of tests discussed in previous paragraphs, will be difficult to achieve. Nonetheless, an attempt was made to advance

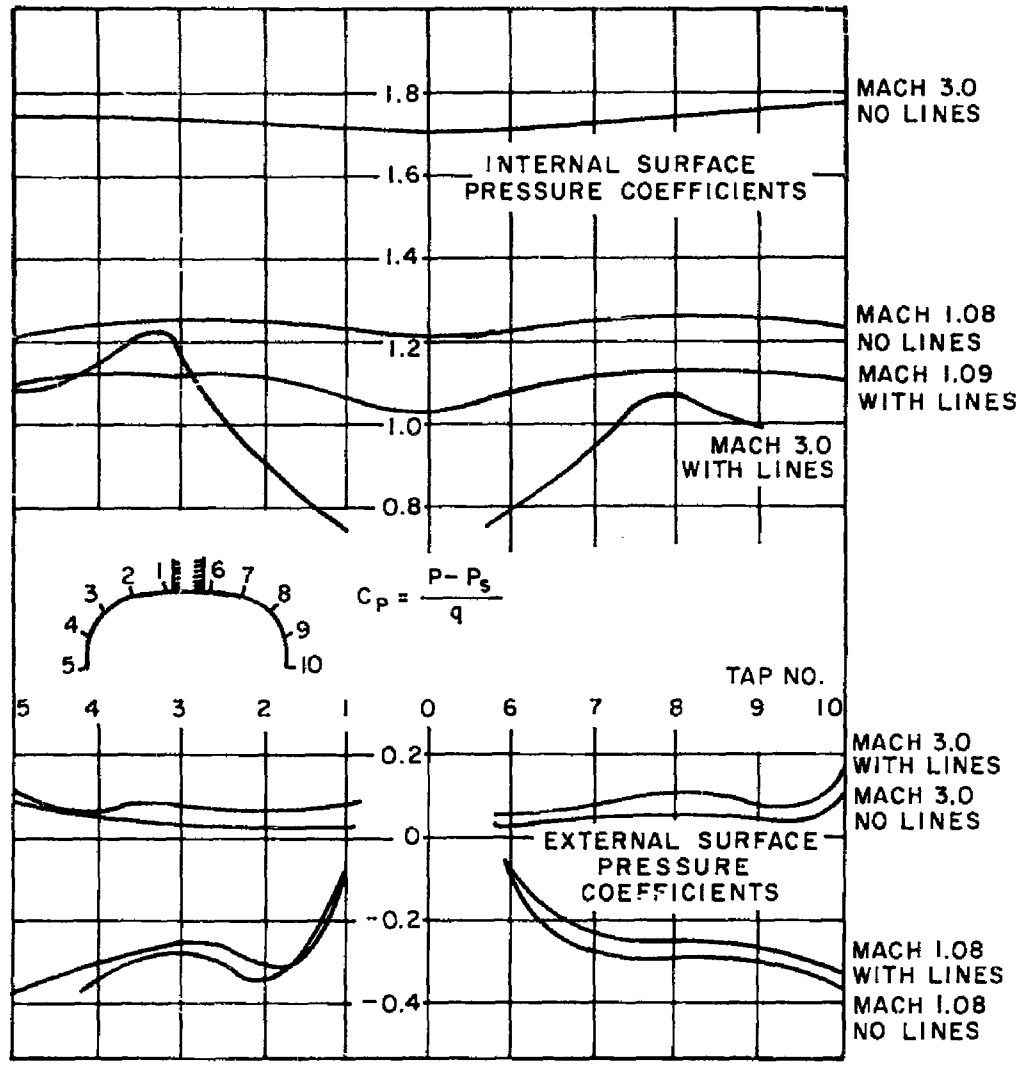

Figure 20. Pressure Coefficient Distribution of a 26% Porosity Ribbon-Type Canopy Model With and Without Suspension Lines, No Forebody

the state-of-the-art of supersonic parachute operations by changing the shape of the parachute canopy. Operation has been extended more than one Mach number by this means.

A detailed analysis was made of results of all tests conducted on flexible, flat, circular, ribbon-type parachute canopies with standard suspension-line lengths of 1 D_o in supersonic flow. This analysis showed that the skirt band and the lower ribbons tend to align themselves at an angle of approximately 14 degrees to the airflow. Thus, the included angle between the suspension lines was approximately 28 degrees, as compared to 40 degrees at subsonic flow. This apparent alignment to a specific angle of attack seemed to indicate that the parachute canopy assumed a shape for which the airflow and pressure conditions may be more favorable. The diameter of the inflated canopy, therefore, was reduced accordingly.

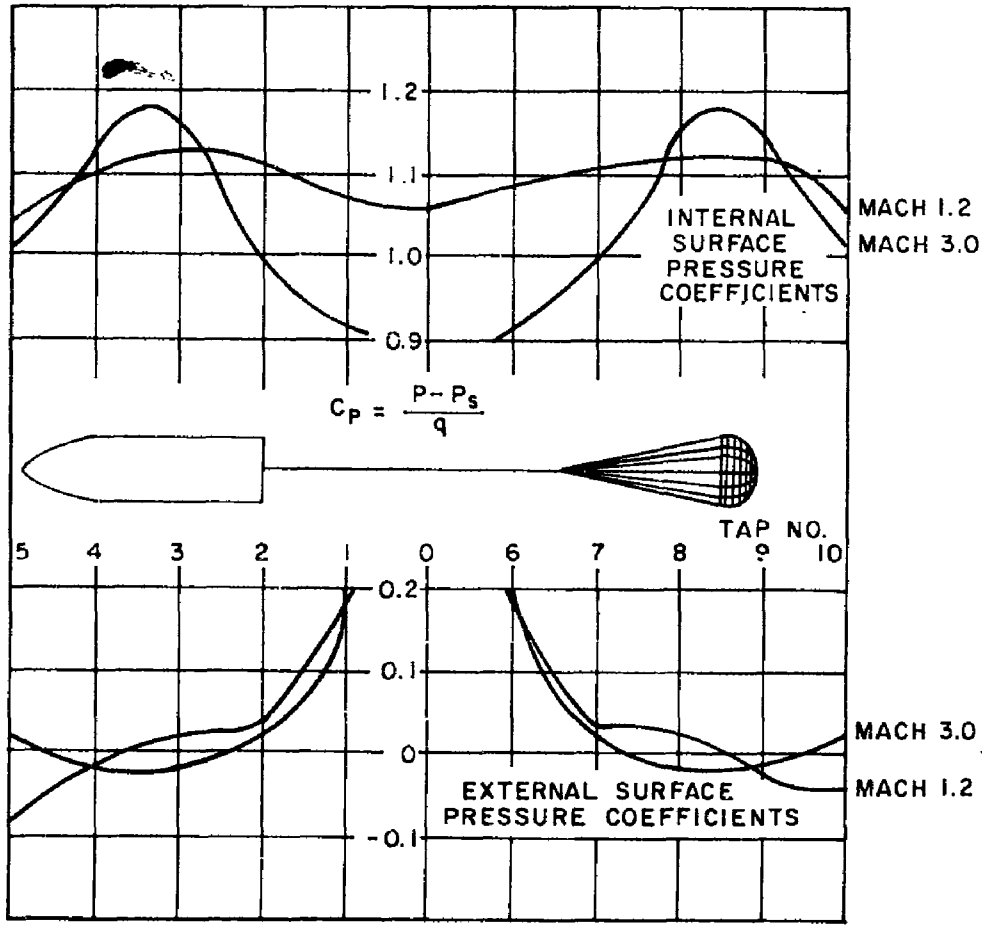

Figure 21. Pressure Coefficient Distribution of a 26% Porosity Ribbon-Type Canopy Model With Suspension Lines and Forebody

The analysis also indicated another phenomenon was detrimental to parachute performance: local flutter, primarily of the lower ribbon material, could become so severe as to damage the entire canopy. This local flutter condition was thought to be due to two factors: (1) excessive ribbon material between the radial ribbons, which causes scallops to form on the canopy, and (2) the instability of a flat plate; each ribbon becomes a flat plate when immersed into an airstream. This latter factor is especially true under conditions of constantly changing angles of attack due to fluctuations of the entire canopy.

These two factors led to a modification of the shape of the flat, circular, ribbon-type canopy by extending the skirt of the canopy along the suspension lines by about 10 percent. In addition, the length of the suspension lines was extended to 2 D_o. This modification altered the shape of the inflated canopy to approximate the shape which the flat, circular canopy tended to assume in supersonic flow, and shortened the free length of the horizontal ribbons in the vicinity of the skirt substantially.

Initially, the triangular gore of a flat, circular ribbon-type parachute canopy was taken as the basic design, and a conical extension, consisting of 10 percent of the canopy constructed diameter, was added. This resulted in the so-called Equiflo (10 percent extended skirt) ribbon-type parachute canopy. Later, the gores were shaped, resulting in the so-called Hemisflo (210° hemispherical) ribbon-type parachute canopy. Gore patterns for both canopy types are shown in Figure 22. Since most of the performance data obtained to date were on the Hemisflo ribbon-type parachute canopy, only these data are reported.

A number of free-flight tests have been conducted on Hemisflo ribbon-type canopies of 2.18 and 4.12 ft. diameter (D_o). These canopies were deployed behind a primary body measuring 9 inches in diameter, at supersonic velocities, and at altitudes between near sea level and 72,000 ft. (Ref. 9).

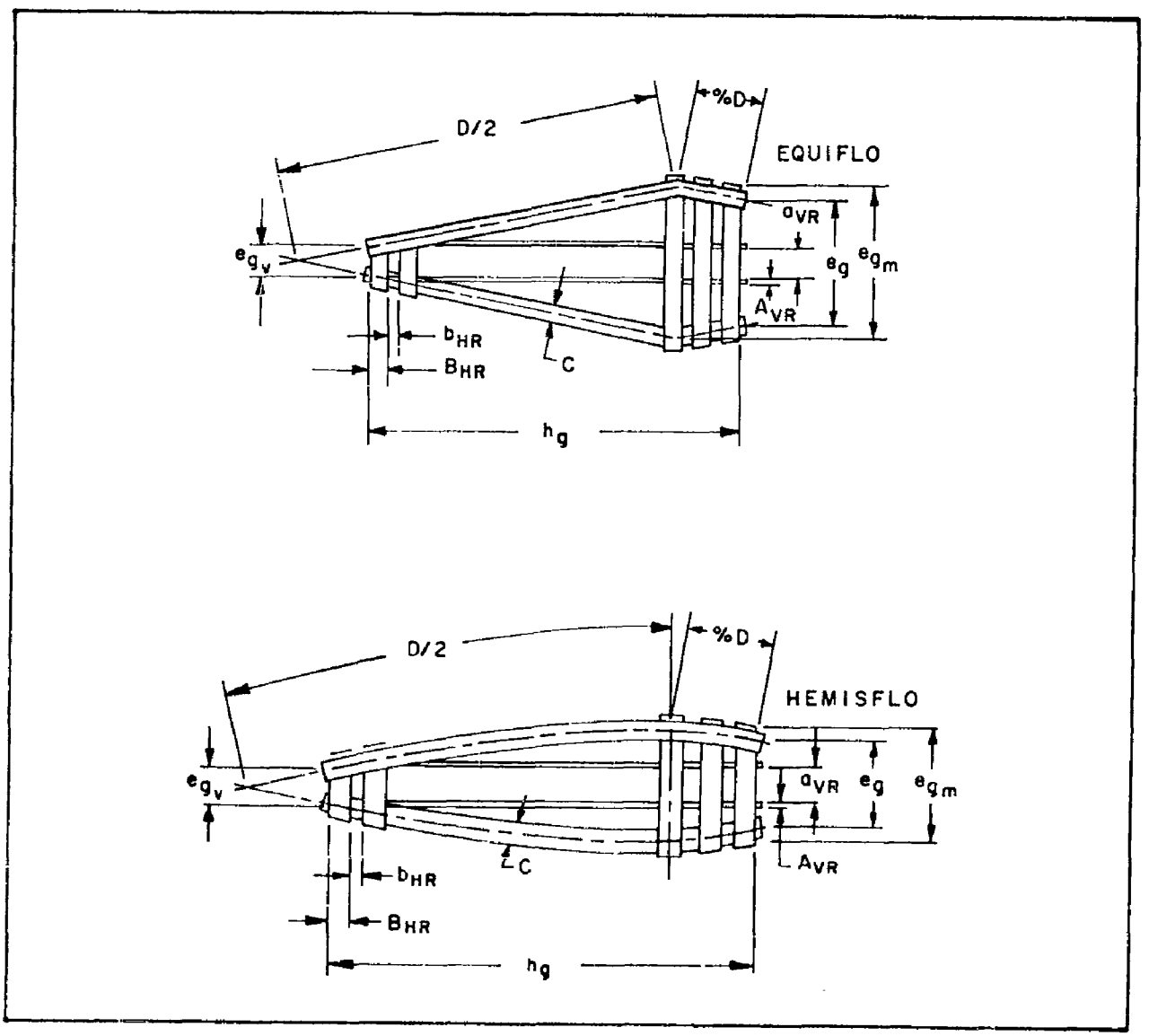

Figure 22. Gore Pattern for Equiflo and Hemisflo Type Ribbon Canopies

The drag coefficient, C_{D_o}, versus Mach number for this type of parachute canopy is plotted in Figure 23. The Hemisflo parachute shows a definite dependence of drag coefficient upon Mach number. The curve for C_{D_o} drops sharply after sonic velocity is exceeded, but seems to begin leveling off in the region above Mach 1.5. Drag coefficient values obtained from wind-tunnel tests of models of equivalent size are also shown for comparison. At subsonic velocities, the drag coefficient of the Hemisflo ribbon-type canopy is somewhat lower than that of the flat circular, ribbon-type canopy because the cloth area is greater and the inflated diameter is slightly lower.

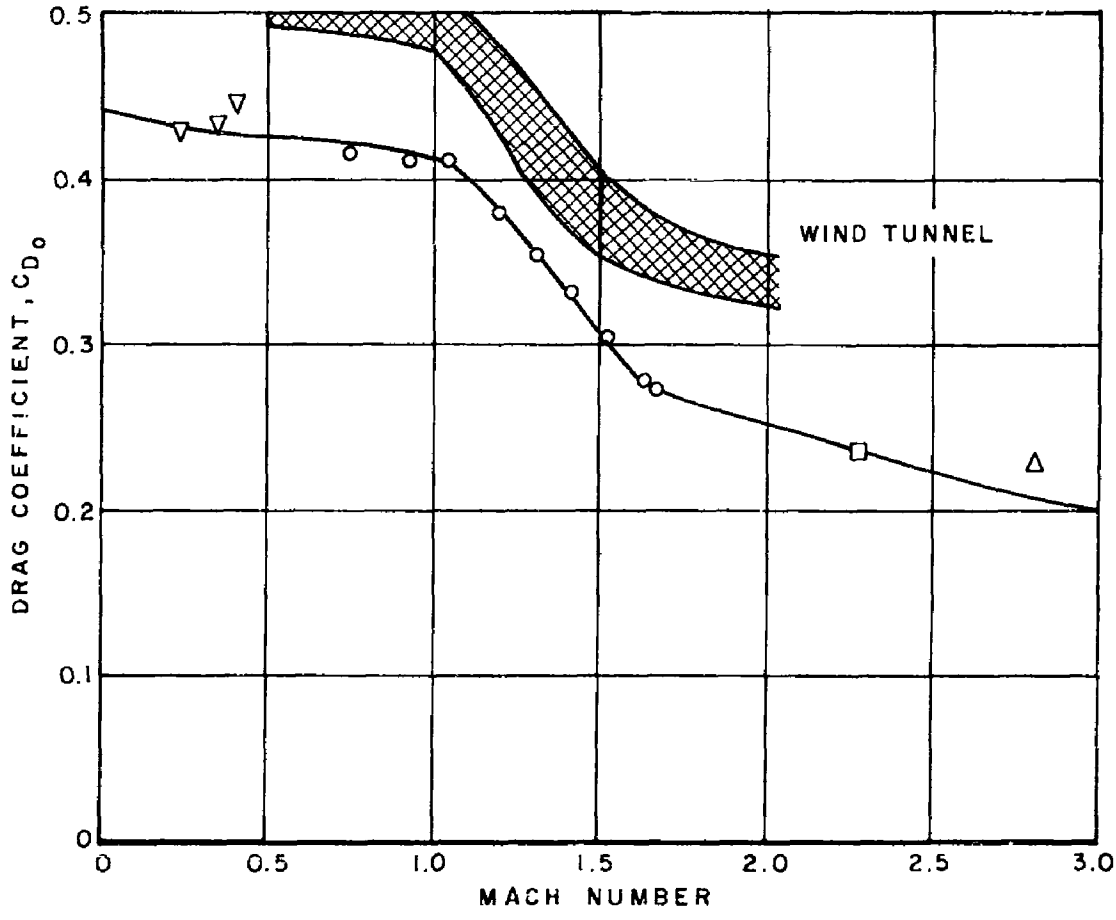

Figure 23. Drag Coefficient Versus Mach Number for Hemisflo Type Parachute Canopy

Drag coefficient values versus Reynolds number and dynamic pressure are plotted in Figures 24 and 25, respectively. The reduction in drag coefficient at speeds greater than Mach 1.0 is obviously due, in part, to the accompanying reduction in inflated area. A closer examination of the test results, however, reveals that other factors must contribute to the reduction. The curves in Figure 23 show a marked resemblance to the plots of drag coefficient versus Reynolds number and dynamic pressure. The shape of these curves with decreasing values of drag coefficient for increasing Mach number corresponds to the shape of curves for increasing Reynolds number and dynamic pressure. All curves for subsonic conditions, however, lie on a straight line, essentially, regardless of the value of either Reynolds number or dynamic pressure. Thus, we conclude that the decrease in drag coefficient with increase in either Reynolds number or dynamic pressure is a Mach number effect. No conclusions as to the effects of either of these parameters upon drag coefficient at supersonic conditions, however, can be drawn.

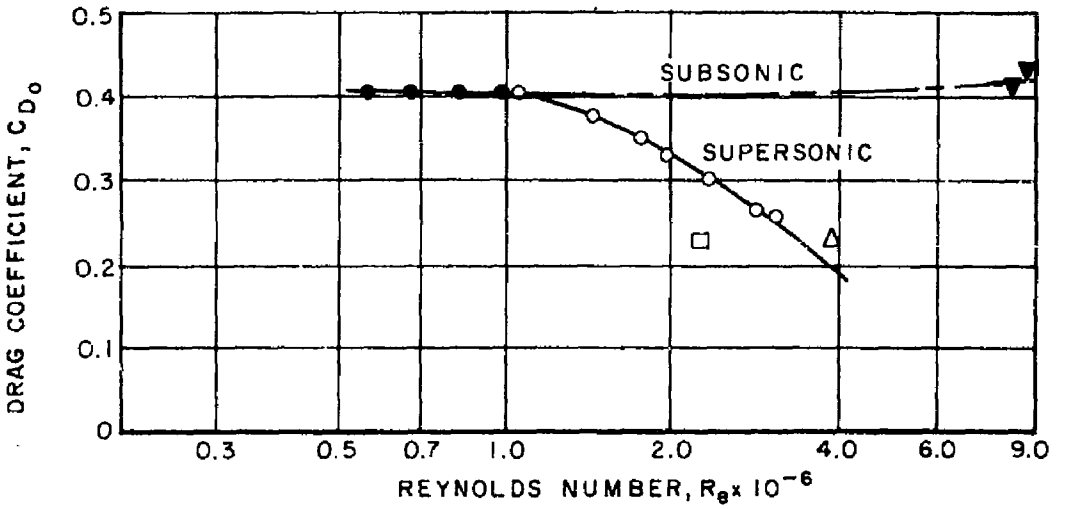

Figure 24. Drag Coefficient Versus Reynolds Number for Hemisflo Type Parachute Canopy

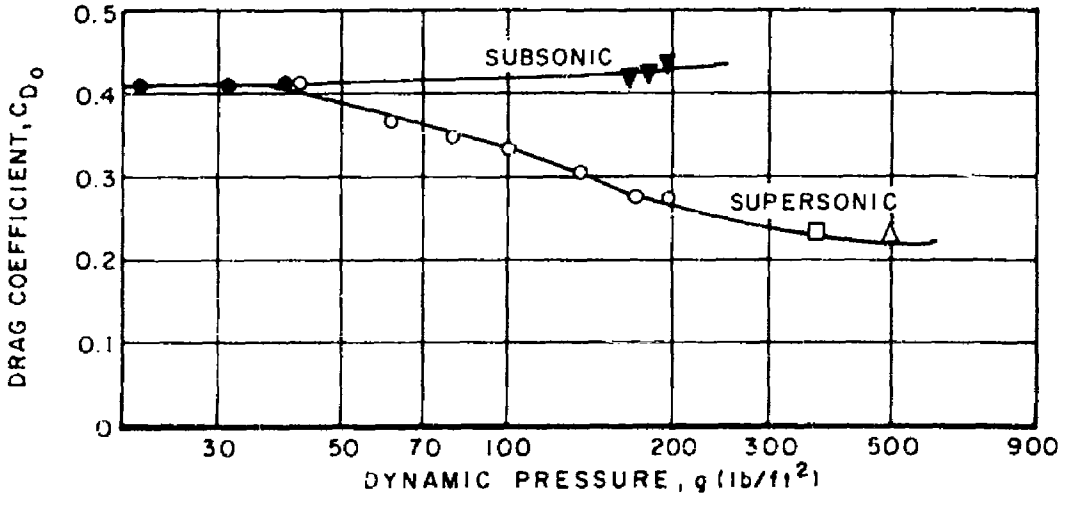

Figure 25. Drag Coefficient Versus Dynamic Pressure for Hemisflo Type Parachute Canopy

A plot of drag coefficient versus area ratio is shown in Figure 26. This curve, compared with a similar plot for a flat, circular, ribbon-type canopy, exhibits the same tendencies, but the rise is much steeper in the sonic region. Approximate Mach number levels are indicated. The curve intersects the fully inflated line (A_R = 0.387) at a drag coefficient value of 0.435, which agrees with the intercept value of Figure 23. No variation of drag coefficient with change in altitude could be detected.

During earlier tests of ribbon-type parachute canopies, some dependency of the area ratio versus Mach number was noted. Inflated area ratio is defined as the ratio of instantaneous projected canopy area, S_{p_i}, to nominal canopy area, S_o. Figure 27 shows a definite dependence of inflated area ratio upon Mach number for the Hemisflo ribbon-type canopy. As Mach number approaches zero, the value of the area ratio approaches a maximum of 0.387, the theoretical maximum area ratio for this canopy type.

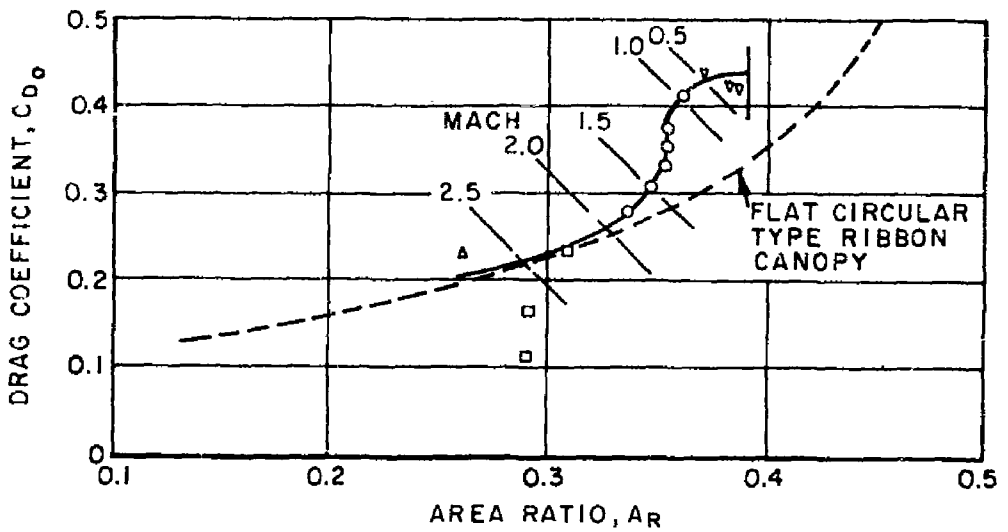

Figure 26. Drag Coefficient Versus Area Ratio for Hemisflo Type Parachute Canopy

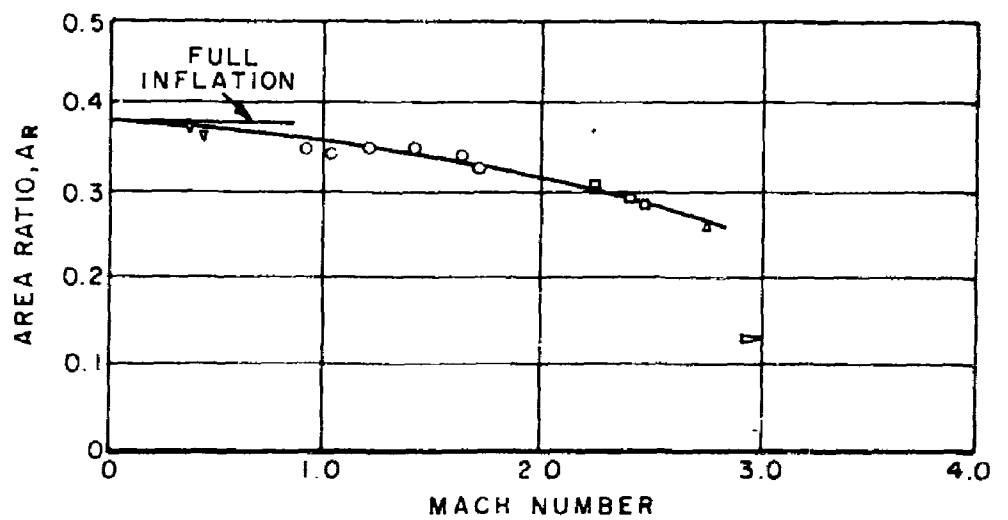

Figure 27. Inflated Area Versus Mach Number for Hemisflo Type Parachute Canopy

The relationships of inflated area ratio versus Reynolds number and dynamic pressure are shown in Figures 28 and 29, respectively. Here again, as in the case of the drag coefficient, the decrease in area ratio with increase in either Reynolds number or dynamic pressure is due, primarily, to Mach number effects. At subsonic conditions, Figure 28 shows practically no change in area ratio over a relatively wide range of Reynolds numbers. However, as soon as sonic velocity is exceeded, a sharp drop occurs. The same is true for area ratio versus dynamic pressure, although the range of dynamic pressures is fairly limited.

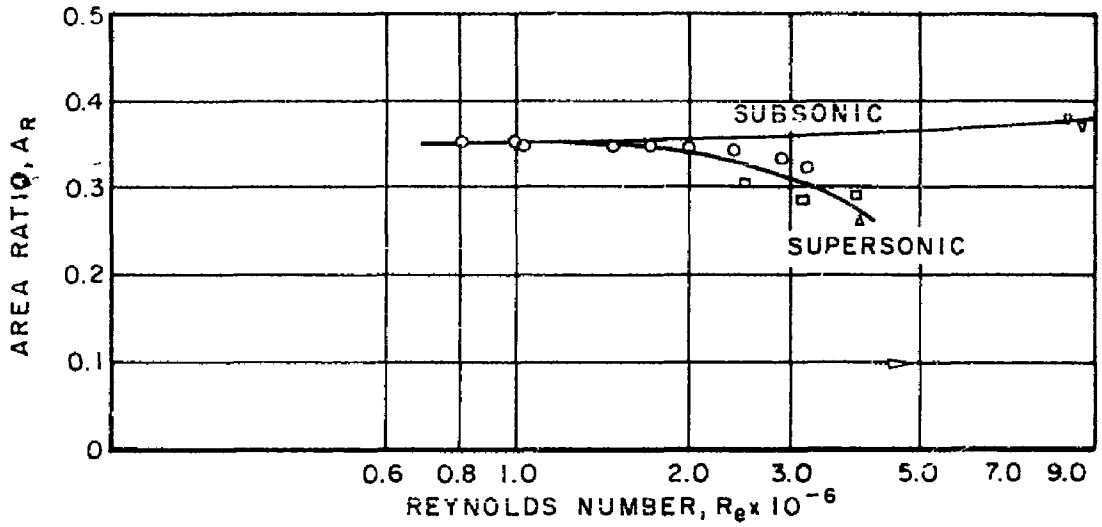

Figure 28. Inflated Area Versus Reynolds Number for Hemisflo Type Parachute Canopy

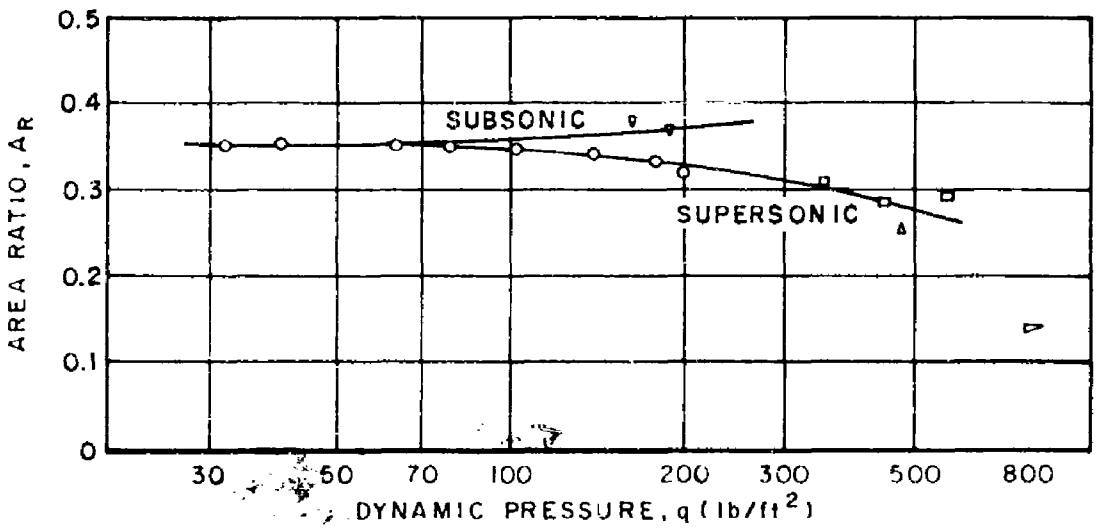

Figure 29. Inflated Area Versus Dynamic Pressure for Hemisflo Type Parachute Canopy

In general, the Hemisflo ribbon-type canopies were relatively stable over a wide range of aerodynamic parameters. Average oscillations were generally less than five degrees from the forebody axis. Canopy filling times agreed well with theoretical considerations, which show that the filling time is essentially independent of air density as long as the orifice coefficient of the material is independent of Reynolds number. Such a dependency exists for solid cloth parachute canopies, as shown by Heinrich (Ref. 10); however, this dependency would be small for geometric-porosity-type parachute canopies. All data available on the ribbon-type parachute canopies, including the Hemisflo type, was plotted as the ratio of filling time to nominal canopy diameter versus velocity at time of snatch (Ref. 4). The resulting curve can be approximated by the expression $\frac{0.65\,\lambda_g}{v_s}$, where λ_g is the geometric porosity and v_s is the snatch velocity. Data correlate satisfactorily when density variation is neglected entirely and the inherent variability of filling is considered. Consequently, we must conclude that the effect of density ratio on filling time for ribbon-type parachute canopies is relatively small. Recent test data, however, indicate some correlation with the fifth root of the density ratio, but more data are required, before this correlation can be firmly established.

CONCLUSIONS

Conventionally shaped and constructed textile parachute canopies are not suitable for reliable and predictable operation in high supersonic flow. A severe aero-elastic problem exists during supersonic operation of conventionally shaped canopies which results in considerably reduced drag and severe damage to structural components. This erratic canopy behavior is believed due, primarily, to the change in pressure distribution on the drag-producing surface with increasing Mach number and the peculiar airflow and shock-wave pattern ahead and inside of the inflated canopy.

Operational capabilities of textile parachute canopies have been extended by approximately one Mach number by modifications to the shape of the original flat, circular, ribbon-type parachute canopy, resulting in the so-called Equiflo and Hemisflo type canopies. Performance characteristics for these types of canopies at Mach numbers up to 2.5 can be predicted. An analysis has shown, however, that extending the operational capabilities of this more- or-less conventionally shaped canopy further would be either extremely difficult or impossible, particularly if the canopy has to operate in essentially undisturbed flow. Consequently, new approaches must be developed to provide satisfactory self-inflating canopy shapes for operations at higher supersonic speed.

In general, the parachute canopy produces drag by changing the momentum of the air through which it passes. In subsonic and, to a certain extent, in transonic operation, the drag-producing surface captures large amounts of air that is accelerated to the terminal or descent velocity of the parachute canopy. This system, consisting of parachute canopy and captured "dead air," passes rather smoothly through free-stream air. Pressure of the captured air is essentially constant within the drag-producing surface, and no significant spillage or violent motion of air within the inflated drag-producing surface results. Tests in supersonic flow, however, indicate that the same parachute canopy does not collect "dead air" within the drag-producing surface; rather, the canopy constantly captures and rejects the air because tremendous energy is associated with supersonic flow. Since the drag-producing surface is inherently flexible, the canopy is distorted according to the movement of the air inside the canopy and a resulting breathing and pumping action occurs.

A careful analysis of supersonic operation indicates that it is difficult, if not impossible, to change the momentum of the air by carrying the entire mass along with the parachute canopy. A means must be found, therefore, which would either change the momentum of the air by a series of smaller pressure changes and flow deflections or which would allow the air to escape through an enlarged vent hole so that only a portion of the available energy would be used. Research efforts along these general lines are being pursued, and initial tests appear promising.

LIST OF REFERENCES

1. United States Air Force Parachute Handbook, WADC TR 55-265, Wright-Air Development Center, W-PAFB, Ohio. December 1956

2. Meyer, R. A., Wind Tunnel Investigation of Conventional Types of Parachute Canopies in Supersonic Flow, WADC TR 58-532. Cook Research Laboratories for Wright Air Development Center. December 1958

3. Engstrom, B. A., Performance of Trailing Aerodynamic Decelerators at High Dynamic Pressures, Phase II, WADD TR 58-284, Part II. Cook Research Laboratories for Wright Air Development Division. March 1960

4. Fredette, R. O., Parachute Research Above Critical Aerodynamic Velocities, Cook Research Laboratories, May 1961. (Unpublished report)

5. Heinrich, H., et al., Progress Reports, Contract AF33(616)-6372, University of Minnesota, January 1960 to June 1961

6. Heinrich, H. G., Ballinger, I. G., Ryan, P. E., Pressure Distribution in Transonic Flow of Ribbon and Guide Surface Parachute Models, WADC TN 59-32. University of Minnesota for Wright Air Development Center, W-PAFB, Ohio. February 1959

7. Engstrom, B. A., Performance of Trailing Aerodynamic Decelerators at High Dynamic Pressures, Phase III, WADD TR 58-284, Part III. Cook Research Laboratories for Wright Air Development Division, W-PAFB, Ohio. December 1960

8. Supersonic Tests Conducted at the Cook Technological Center Wind Tunnel on Parachute Type Decelerator Models. Cook Research Laboratories. October 1960 (Unpublished report)

9. Engstrom, B. A., Performance of Trailing Aerodynamic Decelerators at High Dynamic Pressures, Phases V and VI. WADD TR 58-284, Part V. Cook Research Laboratories for Aeronautical Systems Division, W-PAFB, Ohio. March 1961

10. Heinrich, H. G., Some Research Efforts Related to Problems of Aerodynamic Deceleration. WADD TN 60-276. University of Minnesota for Wright Air Development Division, W-PAFB, Ohio. November 1960

Aeronautical Systems Division, Dir/Aeromechanics, Flight Accessories Lab, Wright-Patterson AFB, Ohio.
Rpt Nr ASD-TDR-62-236. SUPERSONIC PARACHUTE RESEARCH. Final report, May 62, 34p. incl illus., tables, 10 refs. Unclassified Report

Supersonic vehicles require aerodynamic deceleration systems that will function efficiently and predictably at supersonic speeds over a wide range of altitudes. Deceleration from supersonic speeds at high altitudes involves problems that require new approaches. To meet these greater requirements, extensive applied research is being conducted in the field of aerodynamic deceleration.

(over)

This research is expected to provide information for designing adequate deceleration devices that will perform consistently so that recovery trajectories can be predicted.
Parachute canopies are being investigated since parachutes normally provide a high ratio of aerodynamic drag to weight and bulk. Reliable data exist for Guide-Surface and Flat Circular Ribbon parachute canopies at transonic speeds and dynamic pressures as great as 2500 lb/ft^2. At supersonic speeds, however, inflation has been erratic, drag forces reduced, and materials failed at a fraction of rated strength. Probable causes for this erratic behavior are discussed and promising modification and designs of parachute canopies for supersonic operation are presented.

1. Parachutes
2. Fluid mechanics
3. Re-entry aerodynamics

I. AFSC Project 6065, Task 606505
II. R. J. Berndt
III. In ASTIA collection
IV. Not aval fr OTS